The role of syndecans in pathological protein aggregation

Anett Hudák

PhD Thesis

Doctoral School of Theoretical Medicine

University of Szeged

Szeged

2025

I. **Contribution of syndecans to cellular internalization and fibrillation of amyloid-β(1–42)**

a. *Letoha, Tamás; Hudák, Anett ; Kusz, Erzsébet ; Pettkó-Szandtner, Aladár ; Domonkos, Ildikó ; Jósvay, Katalin ; Hofmann-Apitius, Martin, Szilák, László*

Scopus – Multidisciplinary SJR indicator: D1

IF: 3.998

II. **Contribution of syndecans to cellular uptake and fibrillation of α-synuclein and tau**

Hudak, Anett ; Kusz, Erzsebet ; Domonkos, Ildiko ; Josvay, Katalin ; Kodamullil, Alpha Tom ; Szilak, Laszlo ; Hofmann-Apitius, Martin ; Letoha, Tamas

Scopus – Multidisciplinary SJR indicator: D1

IF: 3.998

III. **The Interplay of Apoes with Syndecans in Influencing Key Cellular Events of Amyloid Pathology**

Hudak, Anett ; Josvay, Katalin ; Domonkos, Ildiko ; Letoha, Annamaria ; Szilak, Laszlo; Letoha, Tamas

Scopus - Molecular Biology SJR indicator: Q2

IF: 6.208

IV. **Syndecan-3 as a Novel Biomarker in Alzheimer's Disease**

Hudák, Anett ; Letoha, Annamária ; Vizler, Csaba ; Letoha, Tamás

Scopus - Molecular Biology SJR indicator: Q2

IF: 5.6

V. **Endocytic Pathways Unveil the Role of Syndecans in the Seeding and Spreading of Pathological Protein Aggregates: Insights into Neurodegenerative Disorders**

Hudák, Anett; Letoha, Tamás

Scopus - Molecular Biology SJR indicator: Q2

IF: 4.9

Table of Contents

List of abbreviations

AD- Alzheimer's disease

PD- Parkinson's disease

SDC- syndecan

HSPGs- heparan sulfate proteoglycans

GAG- glycosaminoglycan

HS- heparan sulfate

CS- chondroitin-sulphate

L-syn (α-syn)- L-synuclein (alpha-synuclein)

Trf- transferrin

WT K562- wild type K562 cell

WT SH-SY5Y- wild type SH-SY5Y cell

DIF-SH-SY5Y- differentiated SH-SY5Y cell

UD-SH-SY5Y- undifferentiated SH-SY5Y cell

FLOT1- flotillin 1

FLOT2- flotillin 2

FL- flotillin

CLSM- confocal laser scanning microscope

MOC- Mander's overlap coefficients

SEM- standard error of the mean

CO-IP- co-immunoprecipitation

APC- allophycocyanin

FITC- fluorescein isothiocyanate dye

ThT- Thioflavin-T dye

DAPI- 4 ′, 6-diamidino-2-fenilindol

NaClO3- sodium chlorate

PBS- phosphate-buffered saline

Aβ1-42- amyloid-beta peptide 1-42

CBD- cell binding domain

HSA- HS attachment site

SDS-PAGE- Sodium dodecyl-sulfate polyacrylamide gel electrophoresis

GFP-green fluorescent protein

Abstract

Neurodegenerative diseases such as Alzheimer's disease (AD) and Parkinson's disease (PD) are marked by the pathological aggregation and prion-like spreading of misfolded proteins, including amyloid-beta (Aβ), tau, and alpha-synuclein (α-syn). These proteins undergo structural transitions that lead to oligomer formation, fibrillation, and ultimately neuronal damage. Recent studies suggest that heparan sulfate proteoglycans (HSPGs), particularly transmembrane syndecans (SDCs), are key mediators in the internalization and propagation of these aggregates. However, the isoform-specific roles of syndecans in neurodegeneration remain incompletely characterized.

In this thesis, we systematically investigated the contribution of syndecan isoforms SDC1–4 to the cellular uptake, fibrillation, and intracellular trafficking of Aβ1–42, α-syn, and tau. Using syndecan-overexpressing K562 and SH-SY5Y cells, we employed flow cytometry, confocal microscopy, Thioflavin T assays, scanning electron microscopy, and co-immunoprecipitation techniques. We found that syndecan-3 (SDC3), a neuron-specific isoform, markedly enhanced the uptake and fibrillation of these pathological proteins via a lipid raft-dependent pathway. The heparan sulfate chains of SDCs were critical in mediating this interaction.

Furthermore, we explored the interplay between syndecans and apolipoprotein E (ApoE) isoforms, showing that ApoE2 facilitated, while ApoE4 impaired, SDC-mediated Aβ uptake. Co-localization and biochemical assays confirmed isoform-specific binding between ApoEs and SDCs. SDC3 expression was elevated in human neuronal models and transgenic AD mouse brains, supporting its potential as an early biomarker.

Our findings reveal that syndecans—particularly SDC3—play a central role in the endocytic uptake and seeding of misfolded proteins, contributing to neurodegenerative disease progression. These results highlight the potential of targeting syndecan-mediated pathways for early diagnosis and therapeutic intervention in AD and related disorders.

Introduction

Neurodegenerative diseases are among the most significant healthcare challenges of the 21st century [1]. Alzheimer's disease (AD) and Parkinson's disease (PD) are the most common of these, and their occurrence is steadily increasing as a result of the global aging population [2]. The leading cause of dementia worldwide is Alzheimer's disease, the most common form of dementia in the elderly, which is associated with characteristic clinical and pathological changes in the central nervous system, including neuronal death, deterioration in memory, thinking, learning, and organization [3]. Currently, apart from late-stage symptomatic therapy, these invariably progressive diseases are untreatable and are increasing in number (currently affecting 55 million people worldwide, expected to reach 76 million by 2030), thus increasing the impact on health systems [4]. In Europe, an estimated 8 million individuals live with dementia, and in Hungary alone, approximately 250,000 people are affected [5]. These figures likely underestimate the actual burden, as many patients remain undiagnosed during the early stages of the disease [6]. In addition to the immense personal and social impact, the economic cost is equally overwhelming: in 2019, the worldwide expense of dementia surpassed USD 1.3 trillion, a figure that is projected to more than double by 2030 [7]. In Europe, the yearly direct and indirect healthcare costs associated with dementia have already exceeded EUR 250 billion [8]. Due to the lack of effective therapies, Alzheimer's disease is currently incurable and AD patients face progressive mental and physical decline [9]. As the currently available symptomatic treatments do not slow or prevent the progression of the disease, the development of early diagnosis of AD is key to detecting the disease at the stage of mild central nervous system (CNS) degeneration [10]. The clinical and societal urgency surrounding these conditions underscores the importance of understanding their molecular underpinnings and identifying early diagnostic markers that enable timely intervention [11]. Early diagnosis of Alzheimer's disease (AD) is of paramount importance in maintaining a patient's mental and physical health in a relatively manageable state for a longer period of time [12] [13]. Therefore, discovering predictive biomarkers is essential for accurate AD diagnostics [14]. The discovery of such biomarkers requires a thorough understanding of the early pathophysiological changes that lead to neurodegeneration, because these changes can predict the onset of the disease when the patient is still in a manageable mental and physical state, thus allowing the use of treatments that can halt the progression of AD [12,15].

A key pathological characteristic of neurodegenerative diseases is the gradual buildup of misfolded proteins in the central nervous system [16,17]. In Alzheimer's disease, the extracellular deposition of amyloid-beta (Aβ) peptides—particularly the aggregation-prone Aβ1–42 isoform—leads to the formation of senile plaques, while the intracellular accumulation of hyperphosphorylated tau results in neurofibrillary tangles [18,19]. In Parkinson's disease, alpha-synuclein (α-syn) aggregates into Lewy bodies within neurons [20]. These proteins, initially soluble and functional, undergo conformational transitions into β-sheet-rich structures that form toxic oligomers, protofibrils, and ultimately insoluble aggregates [21,22]. These aggregated proteins disrupt cellular homeostasis, induce oxidative stress, impair proteostasis, and lead to synaptic dysfunction and neuronal death [23]. Moreover, recent discoveries have revealed that these misfolded proteins can propagate through the brain in a prion-like manner [19,24]. This "seeding and spreading" phenomenon involves the release of pathogenic protein aggregates from donor cells, their uptake by neighboring recipient cells, and the subsequent templated misfolding of endogenous proteins [17] [25] [26]. Central to this propagation process is the mechanism of endocytosis, a fundamental cellular function that governs the internalization of extracellular material [27]. Although endocytosis is crucial for processes like nutrient absorption, receptor recycling, and signal transmission in normal conditions, it can also contribute to neurodegeneration by facilitating the uptake of harmful extracellular protein aggregates [28]. Different endocytosis types exist, such as clathrin-mediated, caveolin-dependent, and lipid raft-associated pathways [29]. Of these, non-canonical, lipid raft-dependent endocytosis is increasingly associated with the internalization of Aβ, tau, and α-syn aggregates [17,30]. After uptake, these aggregates are transported via endosomes and lysosomes, which may be degraded, retained, or translocated to the cytoplasm [31]. Dysfunction of the endo-lysosomal pathways is an early and significant feature of AD, and endocytic abnormalities have been observed in neurons even before the formation of extracellular plaques [17,32].

Heparan sulfate proteoglycans (HSPGs), a family of cell-surface and extracellular matrix macromolecules family, have emerged as critical regulators of protein aggregation and endocytosis [33,34]. HSPGs are a core protein to which linear, sulfated heparan sulfate (HS) glycosaminoglycan chains are covalently attached [35]. These HS chains are highly negatively charged due to their sulfate groups and can interact electrostatically with a wide range of ligands, including growth factors, cytokines, lipoproteins, and aggregation-prone proteins such as Aβ, tau, and α-syn [24,36]. HS chains' fine structure and sulfation pattern determine binding

specificity and biological function [37]. Several studies have demonstrated the colocalization of HSPGs with amyloid plaques and neurofibrillary tangles in AD brains, indicating a direct role in disease pathology [38]. In addition to the syndecans, the glypican family represents the other major group of heparan sulphate proteoglycans (HSPGs), which are anchored at the cell surface through glycosylphosphatidylinositol (GPI) bonds rather than transmembrane domains [39]. Glypicans (GPC1-6) are predominantly expressed during development and are involved in morphogen gradient formation, cell growth, and regulation of synapses [40,41]. In neurodegeneration, glypicans play a role in modulating amyloid precursor protein (APP) processing and influencing Aβ aggregation [42,43]. For example, GPC1 has been shown to bind Aβ and influence its fibrillation kinetics, albeit with different dynamics than syndecans [43,44]. Nevertheless, their localization to lipid rafts and ability to cluster amyloidogenic proteins may still indirectly modulate key pathogenic processes [45].

Within the HSPG family, the syndecans (SDCs) constitute the only known group of transmembrane proteoglycans [24]. Syndecans constitute the primary family of transmembrane proteins, which usually carry several heparan sulphate chains [46]. Two small families of cell-surface heparan sulfate proteoglycans (HSPGs) are present on almost all vertebrate cells and are also found in invertebrates, suggesting a long evolutionary history [5]. The syndecan family consists of four members (SDC1–4), each showing unique, yet somewhat overlapping patterns of expression in different tissues (Figure 1) [46]. SDC1 is mainly found in epithelial and plasma cells, SDC2 is predominantly expressed in mesenchymal tissues like fibroblasts and endothelial cells, SDC3 is mainly present in neural tissues, and SDC4 is broadly expressed across various cell types [19,24,47]. The transmembrane syndecans are type I membrane proteins with three or more glycosaminoglycan chains attached close to their N-terminus (i.e., distal to the cell surface) [48]. They have a similar structural organization: an N-terminal ectodomain, a single transmembrane domain, and a C-terminal cytoplasmic domain (~30 amino acids) [49]. They exhibit a high structural diversity [50]. The extracellular part of the syndecan varies significantly among members of the syndecan family, unlike the transmembrane and cytoplasmic domains, which are highly conserved [49]. Specific contacts between the sulfated regions of GAG chains and the essential parts of the protein allow SDCs to interact with numerous extracellular ligands and to transmit signals from the extracellular space to the cell interior [24,51]. The HS chains of the ectodomain mediate binding to extracellular ligands, including Aβ and other amyloidogenic proteins, while the transmembrane and cytoplasmic domains participate in receptor clustering,

lipid raft recruitment, and downstream signaling [52]. Syndecans are not merely passive receptors but active participants in the internalization of misfolded proteins [53]. Syndecans cluster into lipid rafts upon ligand binding and mediate endocytosis independent of clathrin and caveolin [19,24,54]. This pathway has been shown to facilitate the uptake of a broad range of ligands, including viruses, bacteria, lipoplexes, and cell-penetrating peptides [53]. In the context of neurodegeneration, this lipid raft-dependent endocytosis is exploited by Aβ, tau, and α-syn aggregates to enter cells and avoid degradation [24,55]. Once inside, these aggregates may trigger intracellular seeding, contribute to endo-lysosomal stress, and be released to infect neighboring cells [56,57]. Notably, different syndecan isoforms exhibit varying affinities and uptake kinetics for misfolded proteins, suggesting isoform-specific roles in aggregate processing [57].

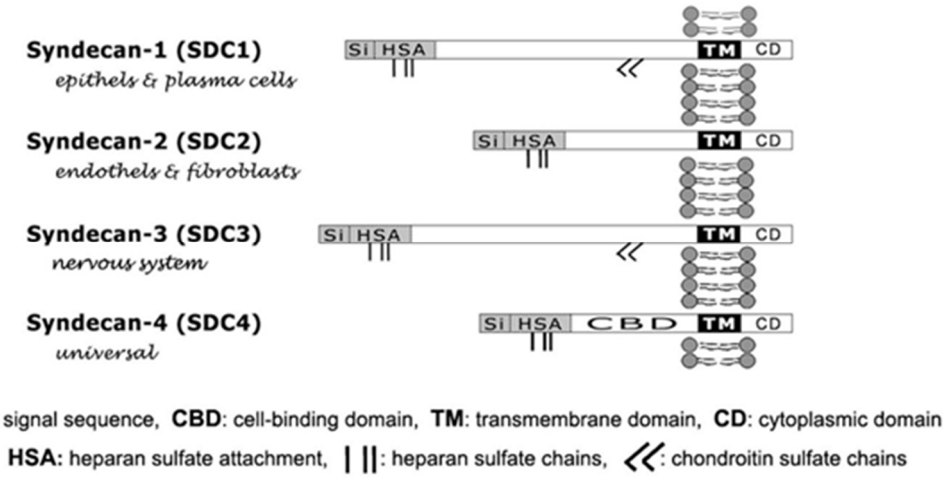

Figure 1. Structural representation of wild-type SDC proteins

Binding to SDCs also promotes oligomerization of the bound ligands, which results from the multivalent nature of the ligand-binding sites of SDCs (i.e., multiple GAG chains, each with numerous ligand-binding sites) and oligomerization mediated by the core protein of SDCs [58,59]. A key feature of the GAG chains of syndecans is that the detailed structure of the heparan sulphate (HS) side chains is determined not by the syndecan isoform itself, but by the cell type in which they are expressed [60] [61]. As a result, the same syndecan isoform may have different ligand-binding properties depending on the cellular environments [60,61]. In addition to GAG-binding sites, SDC3 has several potential O-linked glycosylation sites (resembling a mucin-rich domain), while the SDC4 ectodomain contains a cell-binding domain (CBD) that mediates the cell-cell binding process [62,63]. It appears that SDC-mediated endocytosis occurs in a clathrin-

and caveolae-independent but lipid raft-dependent manner: ligands or specific antibodies induce the aggregation and distribution of SDCs into lipid rafts, thereby stimulating lipid raft-dependent but clathrin- and caveolae-independent SDC core protein endocytosis [19,53,64]. The lipid raft-dependent spreading of α-syn and tau has been previously reported in the literature, while the accumulation of flotillin 1, a lipid raft marker, has been reported in fibrillar degeneration neurons in Alzheimer's disease [19,30,65,66]. Several pathogens and proteins utilize SDC-mediated endocytosis to enter cells, and several macromolecular drug delivery agents, including cell-penetrating peptides and lipoplexes, also use SDCs for cell entry and intracellular transport of cargo [19,67-70]. Recent evidence suggests that α-syn and tau fibrils can spread from one cell to another, inducing neurodegeneration [71,72]. Growing scientific evidence indicates that cell-surface heparan sulfate proteoglycans (HSPGs) play a role in the cellular attachment and subsequent internalization of α-syn and tau fibrils [73-76]. Cell surface heparan sulfate proteoglycans (HSPGs) profoundly influence the cellular uptake of Aβ1-42 by mediating its attachment and subsequent internalization into the cells [19]. Colocalization of amyloid plaques with members of the syndecan family of HSPGs and the increased expression of syndecan-3 and -4 have already been reported in postmortem AD brains [19].

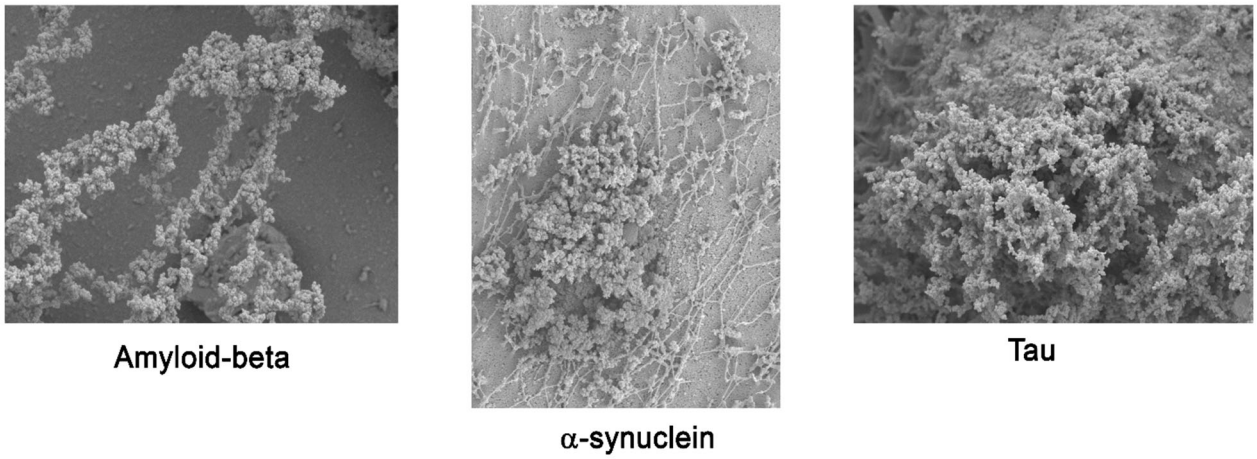

Figure 2. Scanning electron microscope (SEM) image of toxic protein aggregates that play a major role in neurodegeneration.

Considering the growing evidence on the involvement of syndecans in the pathogenesis of AD, we analyzed the contribution of syndecans to cellular uptake and fibrillation of Aβ1-42 (Figure 2) [19]. Among syndecans, the neuron-specific syndecan-3 isoform increased cellular uptake of Aβ1-42 the most [19]. Reviewing the growing scientific evidence on the involvement of syndecans in the pathomechanism of AD, we analyzed the expression of the neuronal syndecan,

syndecan-3 (SDC3), in experimental models of neurodegeneration [12]. Postmortem studies of human AD brains have revealed increased expression of SDC3 and SDC4 in affected regions [12,19,24]. These isoforms also colocalize with senile plaques and neurofibrillary tangles, further implicating them in aggregation [19,77]. SDC3, in particular, is enriched in neurons and appears to be selectively upregulated in regions undergoing early neurodegeneration [12,78]. Beyond their role in protein aggregation, syndecans are also key mediators of inflammation [79]. Their glycosaminoglycan (GAG) chains interact with pro-inflammatory molecules like TNF-α, promoting leukocyte adhesion and their movement out of the bloodstream [80] [12]. In the brain, syndecans present on endothelial cells play a role in the movement of monocytes across the blood-brain barrier, potentially contributing to the development of neuroinflammatory lesions [12].

In addition to syndecans, apolipoprotein E (ApoE) plays a crucial role in Alzheimer's disease [81]. ApoE is a 34 kDa glycoprotein involved in lipid transport and neuronal repair, and it is encoded by three major isoforms: ApoE2, ApoE3, and ApoE4 [82,83]. The ApoE4 variant is the most significant genetic risk factor for late-onset Alzheimer's disease, increasing the risk of developing the condition by up to 14 times [84]. ApoE directly interacts with Aβ and heparan sulfate proteoglycans (HSPGs), including syndecans, through a common heparin-binding region [83]. These interactions affect the clearance, aggregation, and cellular uptake of Aβ [85]. Notably, ApoE4 binds Aβ more strongly than ApoE3 or ApoE2, promoting plaque formation and impairing clearance (Figure 3) [86]. Additionally, ApoE modulates endocytic pathways, potentially influencing the trafficking of Aβ and other molecules internalized via syndecan-mediated pathways [87]. Using our previously established cellular assays for syndecan overexpression, we investigated how ApoE and syndecans' interaction contributes to Aβ pathology's key events, namely uptake and aggregation [83]. The interaction of ApoEs and syndecans suggests isoform-specific features beyond the frequently studied ApoE-heparan sulfate interactions [83].

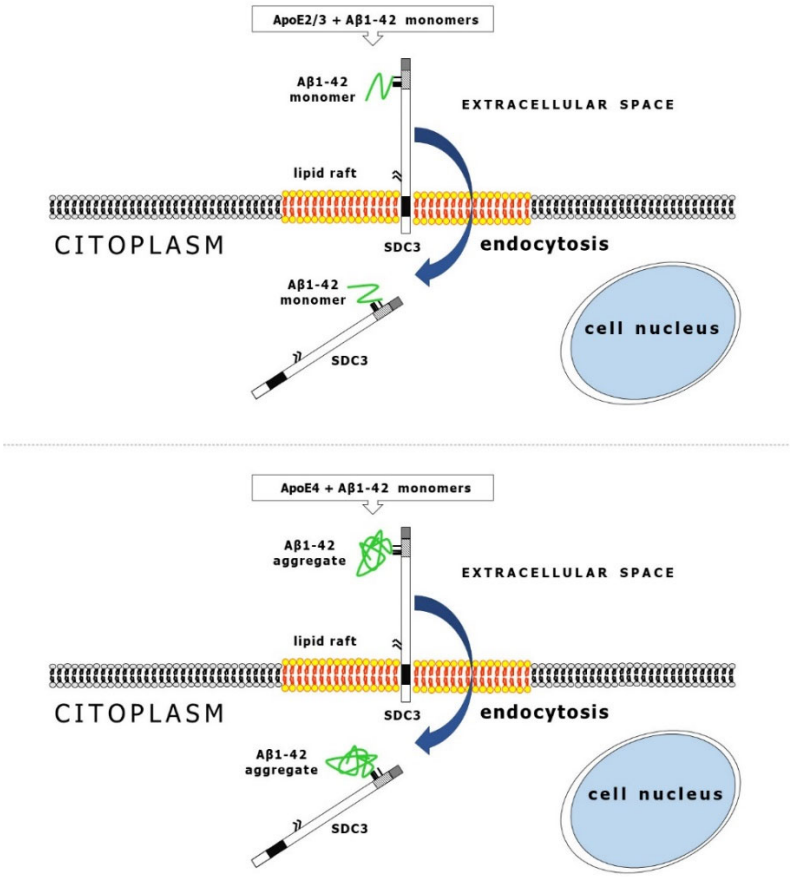

Figure 3. The graphical figure shows that ApoE2 increased the cellular internalization of monomeric Aβ, thus preventing its extracellular aggregation, while ApoE4 decreased it, promoting the formation of extracellular plaques.

These findings place syndecans at a crucial crossroads of amyloid aggregation, endocytosis, inflammation, and genetic risk. Their role in early disease processes, accessibility on the cell surface, and regulated expression make them promising candidates for biomarker discovery [12]. This is particularly significant due to the current absence of reliable biomarkers for detecting Alzheimer's disease in its preclinical stages. Most traditional biomarkers, like cerebrospinal fluid tau and amyloid levels or PET imaging, are indicators of advanced pathology and often involve invasive or costly procedures [88]. In contrast, syndecans, particularly SDC3, can offer a non-invasive, molecularly specific method for detecting early-stage disease [12].

Our results uncover yet unknown details of ApoE cellular biology and deepen our molecular understanding of the ApoE-dependent mechanism of Aβ pathology [83]. The data collected thus clarify the contribution of SDCs in the "seeding and spreading" process of beta-amyloid, α-syn,

and tau, and how they can be used as a potential biomarker for diagnosing Alzheimer's disease. Our results show that overexpression of SDCs, regardless of their cellular source, can trigger fundamental molecular events in the pathology of aggregation-prone proteins [12,19,24].

This doctoral dissertation is dedicated to the systematic exploration of the role of syndecans in the internalization, intracellular accumulation, and intercellular propagation of protein aggregates associated with neurodegenerative diseases.

Aim

The primary objective of this study is to investigate the role of the syndecans (SDCs), a family of heparan sulfate proteoglycans, in the pathogenesis of Alzheimer's disease (AD) and Parkinson's disease (PD). In particular, this research aims to elucidate how SDCs mediate the lipid raft-dependent endocytosis of misfolded proteins such as amyloid beta (Aβ), tau, and α-syn and their potential contribution to the propagation of neurodegeneration. Furthermore, this work seeks to identify isoform-specific interactions between syndecans and aggregation-prone proteins, examining their distinct roles in aggregate internalization, intracellular seeding and spreading in the CNS. Specifically, our research aims to characterize the structural and functional properties of SDC1-4 concerning Aβ, tau and α-syn uptake; to elucidate the mechanisms of SDC-mediated endocytosis and how ApoE isoforms modify this; and to investigate the expression pattern and subcellular localization of syndecan in physiological and pathological conditions.

Understanding these interactions may uncover novel mechanisms contributing to early disease onset and neurodegeneration. The research will also explore the potential of syndecans as early biomarkers in diagnosing AD and PD, allowing early intervention before irreversible neuronal damage occurs. Ultimately, the goal is to promote the development of new diagnostic tools and therapeutic strategies that can slow or prevent the progression of these debilitating diseases, alleviating the personal and societal burden they cause.

Our research helps to emphasise the dual focus on understanding the mechanisms of neurodegeneration, while highlighting potential clinical applications in diagnostics and therapeutics.

Materials and Methods

SDC constructs, cell culture and transfection

SDC overexpressing transfectants were generated in K562 and SH-SY5Y cells using SDC plasmid DNA [19,24,53,83,89] purchased from Origene. Full-length SDC1-4 and SDC4 deletion mutants were amplified and subcloned into mammalian expression plasmid (pcDNA3, pEGFP) from Clontech [19]. Structural SDC4 mutants were generated by inserting a green fluorescent protein (GFP) into the juxtamembrane region of the extracellular segment, with the signals retained in each case to direct the proteins into the membrane [19]. The human SDC DNA constructs were prepared and transfected into K562 cells using Lipofectamine-2000 transfection reagent to generate stable cell lines expressing stable human SDCs or SDC4 structural mutants [19,53]. Transfections were performed according to the manufacturer's guidelines. After 24 hours, the cells were incubated with selection medium containing 0.4 mg/ml G418 (Sigma) and the selection medium was changed every second day [19]. After 2 weeks, G418-resistant colonies were analyzed for the SDC expression with flow cytometry using APC-labeled antibodies specific for the given SDC isoforms (R&D (all R&D Systems, Minneapolis, MN, USA; SDC1: monoclonal rat IgG1 Clone #359103, cat. no. FAB2780A [19,24,83]; SDC2: monoclonal rat IgG2B Clone #305515, cat. no. FAB2965A [19,24,83]; SDC3: polyclonal goat IgG, cat. no. FAB3539A [12,19,24,83]; SDC4: monoclonal rat IgG2a clone #336304, cat. no. FAB29181A [19,24,83]. In the case of GFP-tagged SDC4 mutants, expression was analyzed using flow cytometry to measure fluorescence intensities of the GFP tags [19]. Thus, colonies exhibiting marked SDC expression were chosen for further studies [19]. The erythroleukemia cell line K562 and its SDC clones were grown as a suspension culture in DMEM/F12 medium (Thermo Fischer Scientific) supplemented with 10% fetal calf serum (FCS; Gibco) at 37 °C in a humidified 5% CO_2-containing air environment [19]. For SDC3 overexpressing SH-SY5Y cells, transfection and selection of SDC3 overexpressing clones were performed the same manner as for K562 transfection. SDC3 overexpressing SH-SY5Y clones, along with WT SH-SY5Y cells, were then grown in Advanced MEM medium (Thermo Fischer Scientific) supplemented with 10% FCS (Gibco) at 37 °C in a humidified 5% CO2 containing air environment [19].

Differentiation protocol of SH-SY5Y cells

SH-SY5Y cells were maintained at 37 °C in humidified air containing 5% CO_2 at an initial density of 10^4 cells/cm^2 in 24 or 8-well plates on culture dishes (Corning) previously seeded with 0.05 mg/ml collagen (Merck) [24]. All-trans-retinoic acid (RA, Sigma) was added the day after dissection in Gibco™ Advanced MEM (Thermo Fischer Scientific) containing 10% FBS at a final concentration of 10 μM [19,24]. The medium was changed every 2 days with fresh RA [90]. After 1 week in the presence of RA, cells were washed three times and incubated with 50 ng/ml BDNF (Sigma) in Advanced MEM (without serum) for 2 days before treatment with α-syn or tau [24]. Neuronal differentiation of cells was confirmed using a neuron-specific human βIII-tubulin antibody (eBioscience™, cat. no. 14-4510-82) and secondary Alexa Fluor 546-labeled goat anti-mouse IgG (H+L) together with a cross-adsorbed secondary antibody (Invitrogen, catalog no. A-11003), followed by visualization of cells under confocal microscopy [24].

Flow cytometry analysis of HS and CS expression

As HS was shown to attach Aβ1–42, α-synuclein, tau and ApoE, HS expression of wild-type (WT) K562 cells, SDC transfectants and SH-SY5Y cells were measured with flow cytometry by using anti-human HS antibody 10E4 epitope (Amsbio, cat.no.: 370255-S) and FITC- or Alexa 647-labeled goat anti-mouse IgG (Sigma, cat.no.: AP127F, SAB4600351) according to the manufacturers' protocols [19,24,83]. SDC transfectants with almost equal HS expression were selected for further uptake studies. SDC transfectants were also assessed for CS expression using monoclonal anti-CS primary antibody (Clone CS-56, Sigma, cat.no.: SAB4200696) and FITC-labeled goat anti-mouse IgG (Sigma, cat.no.: AP127F) according to the manufacturers' protocols [19]. Cell surface expression was then measured by flow cytometry using FACScan (Becton Dickinson) [24]. At least 10 000 events per sample were analysed [12,44].

Flow Cytometry Analysis of Cellular SDC3 Expression

SDC3 expression of SH-SY5Y and hCMEC/D3 cells incubated with or without 5 ng/mL of recombinant TNF-α (cat. no. 210-TA-100/CF, RnD Systems, Minneapolis, MN, USA) for 7 days was measured with an AMNIS FlowSight imaging flow cytometer (Luminex Corporation, Austin, TX, USA) by using APC-labeled anti-human SDC3 antibody (polyclonal goat IgG, cat. no. FAB3539A, RnD Systems) [12]. Goat IgG APC-conjugated antibody (R&D Systems, cat.

no. IC108A) was used as an isotype control [12]. SDC3 expression in mouse primary brain endothelial cells and monocytes was analyzed by flow cytometry imaging using mouse SDC3 antibody and specific monocyte or endothelial markers (CD11b or PECAM-1) [12]. After isolation, the isolated primer cells were immunoprecipitated with primary SDC3 antibody (cat. no.: sc-398194, Santa Cruz Biotechnology, Inc., Dallas, TX, USA) and fluorescently labeled secondary antibody (Alexa Fluor 633-labeled goat anti-mouse IgM, cat. no.: A-21046, Invitrogen, Waltham, MA, USA) [12]. Appropriate cell markers (PBECs: mouse PECAM-1 Alexa Fluor 488 conjugated antibody, cat. no.: FAB6874G, R&D Systems and monocytes: Alexa Fluor 488-labeled CD11b monoclonal antibody, Invitrogen, cat. no.: 53-0112-82) were used to identify PBECs and monocytes [12]. At least 5000 events per sample were analyzed [12]. Appropriate gating was used to exclude cell debris and aggregates. Fluorescence analysis was performed using Amnis IDEAS analysis software [12].

Peptides, Proteins and Fluorescent Labeling

Aβ1–42 (i.e., Aβ1–42 trifluoroacetate salt) and its FITC-labeled derivative (FITC-εAhx-Aβ1–42) or 5-TAMRA and HiLyte Fluor 647 Aβ1–42 trifluoroacetate salt were purchased from BACHEM (Bubendorf, Switzerland; cat. no. H-8146 and H-7666) and AnaSpec, respectively, while recombinant ApoEs were purchased from Peprotech Germany, Hamburg, Deutschland [83]. Aβ1–42 peptides (either unlabeled or fluorescently labeled) were kept lyophilized, while fresh Aβ1–42 solutions were prepared by dissolving the lyophilized Aβ1–42 in DMSO immediately prior to the experiments [83]. FITC-labeled human Trf, the marker of clathrin-mediated endocytosis, was purchased from Thermo Fisher Scientific [19]. Fluorescent labeling of ApoE isoforms was performed with the Pierce™ FITC Labeling Kit according to the manufacturer's instructions (Thermo Fisher Scientific, Waltham, MA, USA, cat. no. 53027) [83]. The calculated yield of the labeling was 4.5 mol dye/ApoE [83]. The even fluorescent labeling of the ApoE isoform was confirmed with spectrophotometry (Metertech UV/VIS) and gel electrophoresis [83]. Recombinant tau-441 (2N4R isoform, purchased from rPeptide) was incubated for 5 days to form fibrils as described by Holmes et al. [73]. Briefly, 10 μM protein, in PBS 1 mM DTT pH 7.4, was mixed with low molecular weight heparin (0.05 mg/ml) and incubated with rotary agitation (400 rpm) at 37 °C for 5 days, while confirming fibrils formation with Thiofavin T (ThT) assays and electron microscopy [24]. Before use, the fibrillization mixture was centrifuged, and the resultant pellet was resuspended in PBS 1 mM DTT, pH 7.4,

without heparin to a stock solution [24]. Formation of α-syn fibrils was induced as described by Ihse et al. [91]. Briefly, α-syn (purchased from rPeptide) was dissolved in PBS to a concentration of 140 μM (~2 mg/ml) and incubated at 37 °C with rotary agitation (400 rpm) for 10 days while monitoring fibril formation with ThT assays and electron microscopy [24]. After 10 days of incubation, the fibril solution was centrifuged at 20,000 × g for 30 min to separate the insoluble fibrils from smaller soluble aggregates and/or monomers [24]. The pellet was re-dissolved in PBS to a stock solution. Concentrations were determined by measuring absorbance using NanoDrop [24]. Labeling of α-syn or tau fibrils was performed with the FITC or Alexa Fluor 633 labeling kits according to the manufacturer's instructions (Thermo Fisher Scientific) [24]. The calculated yield of the labeling was 3.4 mol dye/tau and 2.2 mol dye/α-syn. For all the experiments, only freshly prepared sonicated fibrils (8 pulses of 30% amplitude) or freshly prepared monomers were used [24].

Flow Cytometry Analysis of Cellular Uptake

WT K562 and SH-SY5Y cells, differentiated SH-SY5Y cells, SDC transfectants, and SDC4 structural mutants were used to quantify the internalization of α-syn or tau fibrils, monomeric Aβ1–42, and ApoE [24]. These proteins were fluorescently labeled with FITC or Alexa Fluor 633 [24]. Transferrin labeled with FITC (FITC-Trf) was included as a control for clathrin-mediated endocytosis [24]. Briefly, 6 × 105 cells/ml in DMEM/F12 medium (with 10% FCS) were incubated with the fluorescently labeled (FITC-, or in the case of SDC4 mutants, HiLyte Fluor 647) α-syn, tau, Aβ1–42, Trf or ApoEs (at a concentration of 5uM monomer equivalent and 25ug/ml, respectively), for ApoEs (at concentrations of 5 μM and 500 nM), for various amounts of time (1,3,6 and 18h) at 37°C [24,83]. The effect of ApoEs on Aβ1–42 uptake was measured by preincubating the cells with either of the unlabeled ApoE isoforms for 30 min at 37 °C at a concentration of 500 nM, before treating the cells with 5 μM of FITC-labeled Aβ1–42 [83]. After incubation, the cells were washed twice in ice-cold PBS and progressed towards flow cytometry [83]. In the case of the FITC- or HiLyte Fluor 647-labeled proteins, after incubation and washing, the cells (WT K562, SH-SY5Y, and SDC transfectants) were resuspended in 0.5 ml of physiological saline [19,24]. Equal volumes of this suspension and a stock solution of trypan blue (Merck KGaA; 500 μg/ml dissolved in ice-cold 0.1 M citrate buffer at pH 4.0) were allowed to mix for 1 min before the flow cytometric analyses [19]. In this

way, the sample pH was lowered to pH 4.0, thereby optimizing the quenching effect of trypan blue to quench the extracellular fluorescence of surface-bound fluorescent proteins [19,24,53,83,92]. In the case of the SDC4 mutants treated with Alexa Fluor 633 or HiLyte Fluor 647-labeled proteins, extracellular fluorescence of surface-attached α-syn, tau, or Aβ1–42 was removed by trypsinization according to the method described by Nakase et al. [24] [93]. Cellular uptake was then measured by flow cytometry using FACScan (Becton Dickinson). A minimum of 10,000 events were analyzed for each sample [19,83]. Cell viability in cell suspension was determined by propidium iodide (10 μg/ml) and appropriate gating in the forward scatter-side scatter plot to exclude dead cells, debris, and aggregates [19,53,83].

Microscopic Visualization of Cellular Uptake and Internalization

The internalization of fluorescently labeled Aβ1–42, ApoEs, α-syn, tau fibrils, or monomers (labeled with FITC, Alexa Fluor 633, 5-TAMRA, or HiLyte™ Fluor 647) was visualized using confocal laser scanning microscopy (CLSM) [24,83]. WT SH-SY5Y and K562 cells, along with SDC transfectants and SDC4 mutants, were grown on poly-D-lysine-coated glass-bottom dishes [19]. After 24 hours, the cells were pre-incubated in DMEM/F12 medium supplemented with 10% FCS at 37°C for 30 minutes, followed by incubation with fluorescently labeled Aβ1–42, ApoEs, α-syn, tau, or Trf at concentrations of 5 μM (Aβ1–42, α-syn, tau) or 25 μg/ml (Trf) [19,24,83]. After incubation, cells were rinsed with ice-cold PBS, fixed with 4% paraformaldehyde, and stained with DAPI for 5 minutes [19]. For colocalization studies, after fixation, cell membranes were permeabilized with 1% Triton X-100 and treated with APC-labeled SDC antibodies along with Alexa Fluor®-labeled flotillin antibodies [19,24,83]. The samples were then washed and stained with DAPI again, embedded in Fluoromount G, and fluorescence distribution was analyzed on an Olympus FV1000 confocal microscope using multiple lasers (blue, green, and red channels) [19,24,83]. For visualizing oligomeric Aβ1–42, α-syn, or tau internalization, cells were incubated with fibrils or monomers, treated with Thioflavin T or Congo Red, and fixed, followed by DAPI staining [19,24,83]. Fluorescence was analyzed as described above. Colocalization analyses (SDCs with Aβ1–42, α-syn, tau, or Trf; SDCs with flotillins) were performed using ImageJ with the JACoP plugin or Olympus Fluoview software to calculate Mander's overlap coefficient (MOC) [19,24,83]. A total of 21 images (7 per sample, triplicate experiments) were analyzed, and the data are presented as mean ± SEM [19,24,83].

Animal Experiments and Immunohistochemistry

The in vivo experiments were performed using 12-month-old APPSWE-Tau transgenic mice (Taconic Biosciences, Inc., Germantown, NY, USA) and age-matched C57BL/6 wild-type (WT) controls [12]. Each group (WT and APPSWE-Tau) consisted of 8 mice, with 4 males and 4 females in each group [12]. The animals were anesthetized using 2,2,2-Tribromoethanol (cat. no. T48402, Merck KGaA, Darmstadt, Germany), and blood was collected via cardiac puncture [12]. Following transcardial perfusion with ice-cold PBS (2 mL/min; cat. no. BE17-516F, Lonza, Basel, Switzerland), the brains were removed, frontally dissected, and frozen in dry ice for further analysis using ELISA and microscopic examination [12].

For immunohistochemistry, brain samples from 8 mice per group were fixed for 18 hours in 4% paraformaldehyde (cat. no. P6148, Sigma-Aldrich), then dehydrated in an ethanol series, cleared with xylene (cat. no. 00699464, Avantor Inc., Radnor, PA, USA), and embedded in paraffin (cat. no. 26154.291, Avantor Inc.) [12]. Ten µm thick sections were cut using a microtome (Leica Biosystems Inc., Buffalo Grove, IL, USA) and mounted onto SuperFrost Plus® slides (Thermo Fisher Scientific Inc., Waltham, MA, USA) [12]. Antigen retrieval was performed in 10 mM citrate buffer (pH 6.0) at 95–100°C for 10 minutes, then slides were cooled to room temperature for 20 minutes [12]. The slides were then incubated in a blocking solution (5% goat or donkey serum diluted in 0.1% PBST) at room temperature for 30 minutes [12]. After blocking, the primary antibody (Aβ-specific antibody, MOAB-2, cat. no. NBP2-13075, NOVUS Biologicals, Littleton, CO, USA) was applied at a concentration of 100 µL per slide, diluted in blocking solution (1% BSA or goat serum in 0.1% PBST), after incubated either at room temperature for 1 hour or at 4°C overnight [12]. Following three 10-minute washes with PBST, the slides were stained with 100 µL of Alexa Fluor 488-labeled secondary antibody (cat. no.: A-21141, Thermo Fisher Scientific), diluted in blocking solution, for 1 hour at room temperature [12]. After rinsing the slides three times with PBS, they were covered with cover slips using mounting media [12].

Plaque Load Assessment and Tissue Concentration Measurements

The Aβ plaque load in brain tissue was quantified using morphometric analysis via ImageJ software, measuring the area of amyloid plaques stained with an Aβ-specific antibody [12]. The plaque load was expressed as the percentage of the total area covered by plaques, with two samples per animal analyzed [12]. For TNF-α tissue concentrations, brain samples were homogenized in a lysis buffer with protease inhibitors and analyzed using the mouse TNF-alpha

Quantikine ELISA Kit (R&D Systems) [12]. TNF-α levels were also measured in whole blood from the mice. Similarly, SDC3 tissue concentrations were assessed by homogenizing brain and liver samples and analyzing the lysates with the mouse SDC3 ELISA Kit PicoKine® (BOSTER Biological Technology), following the manufacturer's guidelines [12].

Co-immunoprecipitation experiments

Co-immunoprecipitation (Co-IP) experiments were performed using stable SDC3 transfectants or wild-type SH-SY5Y cells to study protein interactions. Cells were incubated with FITC-labeled α-syn, tau fibrils, Aβ1-42, or ApoEs for 18-24 hours at 37°C, followed by lysis with cold Pierce IP buffer. The lysates were incubated with primary antibodies (SDC3, SDC4, flotillin-1, and flotillin-2) overnight, and antigen-antibody complexes were captured using pre-washed Protein A/G magnetic beads. After elution, the samples were analyzed by SDS-PAGE, and protein complexes were visualized using a UVITEC Alliance Q9 Imager. Band intensities were quantified with NineAlliance software. This method was employed to investigate the interactions between SDC3 and key proteins, such as α-syn, tau, Aβ1-42, and ApoEs, providing valuable insights into the mechanisms of cellular protein binding.

Thioflavin T binding assays

Thioflavin T (ThT) binding assays were used to evaluate the formation of amyloid fibrils in different cell lines. WT K562, SH-SY5Y, and SDC transfectant cells were seeded into 96-well microplates and incubated with Aβ1–42 (5 μM), α-syn, or tau (5 μM) monomers for different time intervals (1, 3, 6, and 18 hours) [19,24,83]. After incubation, ThT (15 μM) was added to the cell cultures 10 min before measurement, and the fluorescence intensity was measured using a multi-mode reader with an excitation wavelength of 440 nm and emission at 480 nm. The fold change in fluorescence intensity, relative to the background ThT signal, was calculated to assess the fibril formation in Aβ1–42, α-syn, or tau-treated cells [94].

Additionally, differentiated WT and SDC3-overexpressing SH-SY5Y cells were treated with ApoE isoforms (500 nM) and then exposed to Aβ1–42 for 3 or 18 hours. The fluorescence was again measured to determine the interaction between ApoE and amyloid fibrils, providing insight into the potential role of ApoE in amyloid aggregation. This approach allowed for the real-time analysis of amyloid fibril formation in cellular models.

Scanning Electron Microscopy of Surface Attachment and Fibrillation

WT SH-SY5Y, K562, and SDC transfectants were cultured on poly-D-lysine-coated glass-bottom dishes. After a 24-hour incubation, cells were exposed to α-syn, tau fibrils, or monomers (5 μM) for various durations (10 min to 18 h), followed by fixation in glutaraldehyde and alcian blue, post-fixation in osmium tetroxide, dehydration, and gold coating. Proteins' fibrillation and surface attachment were examined via scanning electron microscopy (SEM) using a JEOL JSM-7100F/LV microscope [24].

In separate experiments, Aβ1–42 fibrils (5 μM) were incubated with SH-SY5Y and K562 cells, including SDC transfectants and SDC4 mutants, for up to 18 hours. Surface attachment and fibrillation of Aβ1–42 were also analyzed using the SEM technique described above [19].

Furthermore, differentiated SH-SY5Y cells overexpressing SDC3 were treated with ApoE isoforms (500 nM) for 30 minutes before exposure to Aβ1–42 (5 μM) for 3 or 18 hours. SEM imaging was employed to observe the interaction of ApoE and Aβ1–42 and the resultant fibril formation.

Isolation of mouse monocytes and brain endothelial cells

According to the manufacturer's instructions, monocytes were isolated from collected blood samples using the EasySep™ Mouse Monocyte Isolation Kit (Cat. No. 19861, Stemcell Technologies Inc, Vancouver, BC, Canada). Mouse brain endothelial cells were isolated using the method of Assmann et al. [95]. The SDC3 expression of isolated monocytes and primary brain endothelial cells (PBECs) was analyzed by mouse SDC3 antibody and specific monocyte or endothelial markers (CD11b or PECAM-1) using flow cytometry imaging. After isolation, the isolated primer cells were treated with a primary SDC3 antibody (cat. no. sc-398194, Santa Cruz Biotechnology, Inc, Dallas, TX, USA) and a fluorescently labeled secondary antibody (Alexa Fluor 633-labeled goat anti-mouse IgM, cat. no. A-21046, Invitrogen, Waltham, MA, USA). The corresponding cellular markers (PBECs: mouse PECAM-1 Alexa Fluor 488 conjugated antibody, cat. no. A-21046, Invitrogen, Waltham, MA, USA; cat. no. FAB6874G, RnD Systems and monocytes: Alexa Fluor 488-labeled CD11b monoclonal antibody, Invitrogen, cat. no. 53-0112-82) were used to identify PBECs and monocytes [12].

Statistical analysis

Results are expressed as means ± standard error of the mean (SEM). Differences between experimental groups were evaluated using one-way variance analysis (ANOVA). Values of $p < 0.05$ were accepted as significant. Pearson's correlation coefficient was calculated for the correlation between the SDC3 or HS expression and Aβ1–42 uptake and fibrillation values of SH-SY5Y cells. For colocalization analyses, the Mander's overlap coefficient (MOC) was calculated as described by Wesen et al. [96]. Pearson's correlation coefficient was used to measure the strength of a linear association between two variables [12].

Results

Our work investigated the role of syndecans (SDCs) in the uptake and fibrillation of amyloid-β (Aβ1-42). While heparan sulfate proteoglycans (HSPGs) are known to promote cellular binding and internalization of Aβ1-42, the specific contribution of transmembrane SDCs is not fully elucidated [19]. To enable the exact assessment of SDCs' contribution to cellular uptake of Aβ1–42, while minimizing the interfering effects of other HSPGs or caveolae-mediated endocytosis, stable transfectants of SDCs were created in the K562 cells, a cell line with reportedly low HSPG and no syndecan or glypican expression, along with no detectable levels of caveolin-1, the main component of caveolae [19,97-99]. Thus, SDC transfectants with similar levels of HS expression were selected and treated together with wild-type (WT) K562 cells with FITC-labeled Aβ1-42 or transferrin (Trf), a marker of clathrin-mediated endocytosis, for 1, 3, 6 and 18 h [19]. The contribution of SDCs to cellular uptake and binding of FITC-Aβ1-42 or FITC-Trf was quantified by quantitative flow cytofluorometric assays (Figure 4) [19]. Protein internalization was assessed by adding trypan blue (dissolved at 0.25% concentration in ice-cold 0.1 M citrate buffer) 1 min before analysis, thus quenching the extracellular fluorescence of surface-bound fluorescent proteins (Aβ1-42 or Trf) [92]. The extracellularly bound proteins were quantified by the difference in fluorescence measurements between protein-treated, unquenched, and trypan-blue-quenched samples [19]. Flow cytometry analysis showed that SDC3 transfectants showed the highest internalization of Aβ1-42 at all time points, followed

by SDC4, which outperformed wild-type (WT) K562 cells in uptake after 6 h, with SDC2 transfectants also showing increased uptake, but only after 18 h [19]. In contrast, SDC1 showed lower Aβ1-42 uptake at 18 hours [19]. The uptake of transferrin (Trf), a clathrin-mediated endocytosis marker, was higher in WT cells than in most SDC transfectants, suggesting different endocytic pathways for Aβ1-42 and Trf [19].

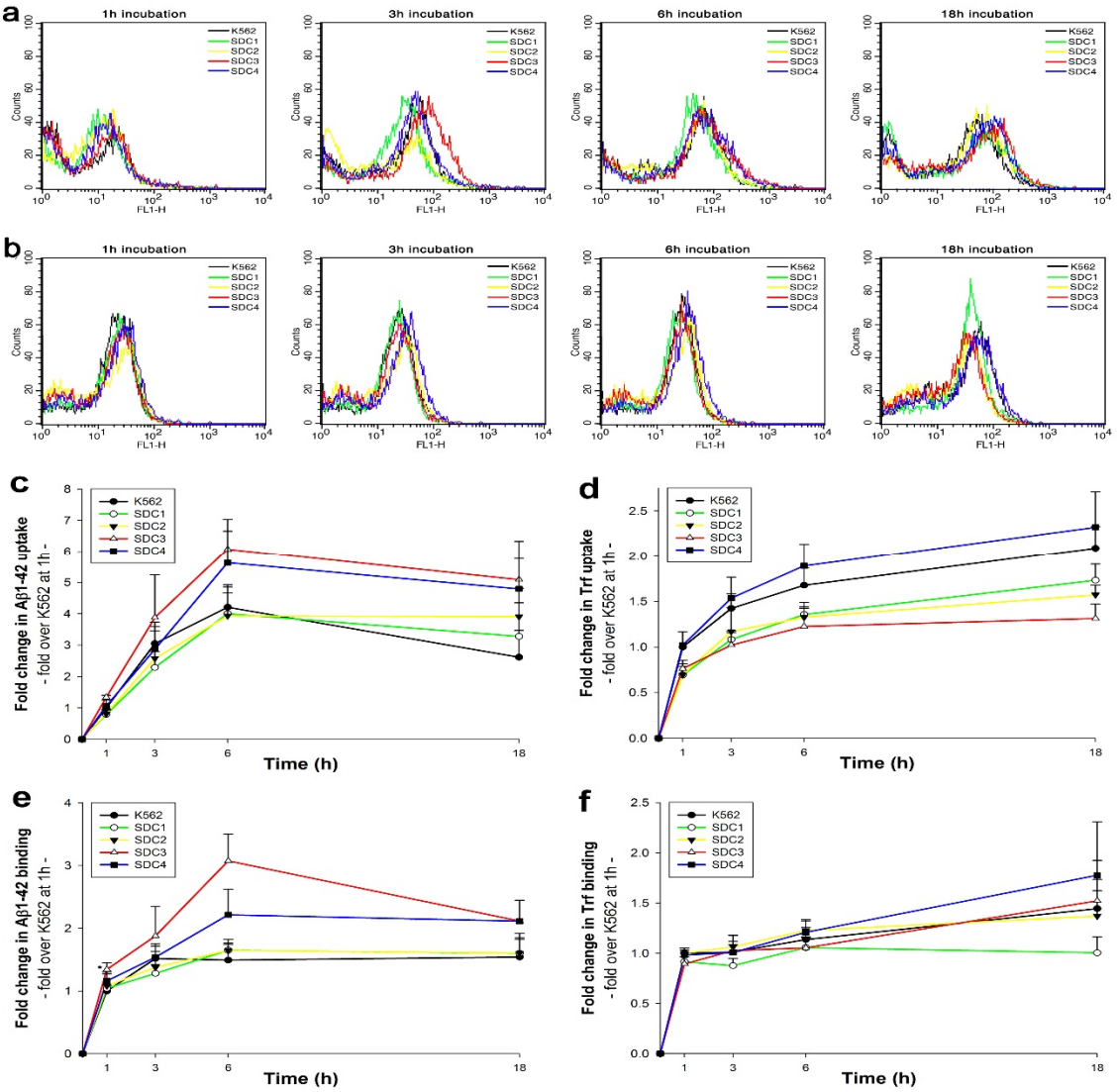

Figure 4. Kinetics of Aβ1–42 and Trf uptake. WT K562 cells and SDC transfectants were incubated with FITC-labeled Aβ1–42 or Trf for 1, 3, 6 and 18 h at 37 °C. Cellular uptake and attachment were analyzed with flow cytometry. (a,b) Flow cytometry histograms showing the kinetics of intracellular fluorescence following incubation with fluorescent Aβ1–42 and Trf, respectively. (c–f) Detected intra- and extracellular fluorescence intensities of Aβ1–42 or Trf-treated cells were normalized to WT K562 cells treated with the respective proteins (either Aβ1–42 or Trf) for 1 h. The lines represent mean ± SEM of four independent experiments.

In studying the fibrillation of Aβ1-42, our ThT fluorescence assays showed that SDC3 and SDC4 significantly ($p < 0.05$) promoted fibrillation of Aβ1-42, which was also demonstrated by our ThT fluorescence assays, confirming that SDC3 and SDC4 promote fibrillation. Our scanning electron microscopy studies also supported this, which showed enhanced fibrillar Aβ1-42 structures on SDC3 and SDC4 transfectants after only 1 h of incubation (Figure 5).

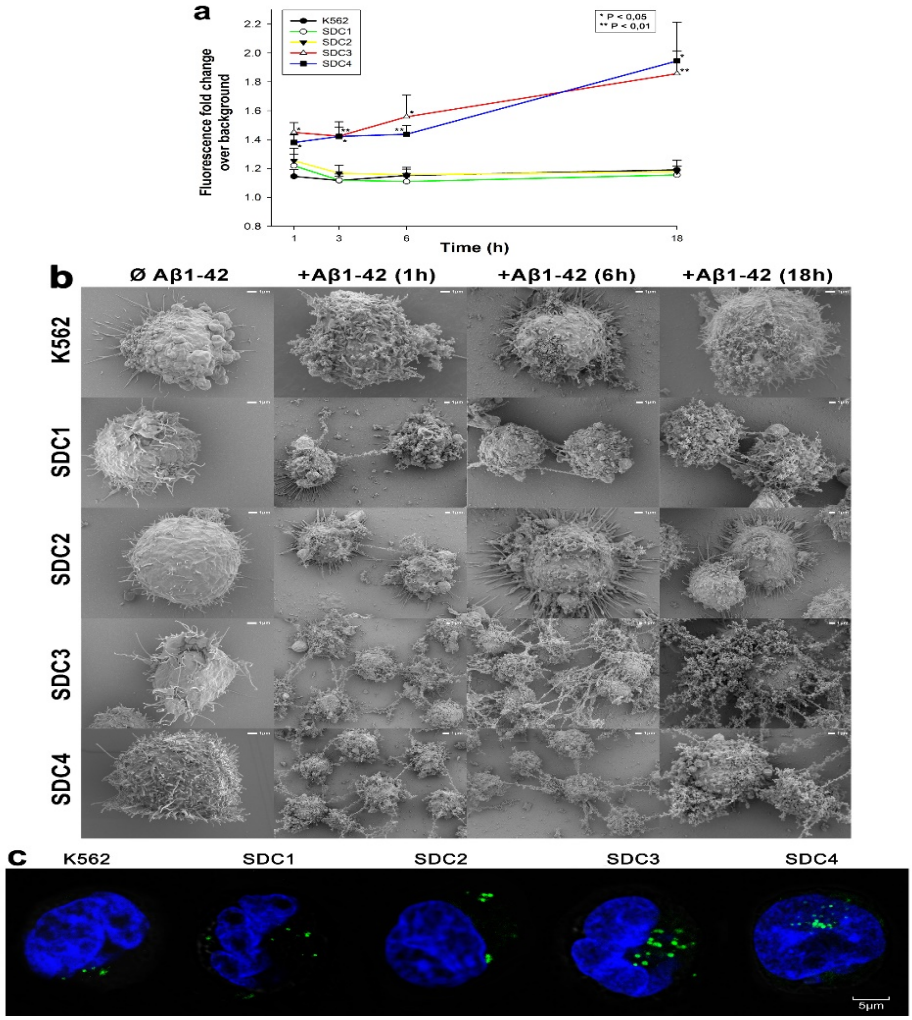

Figure 5. Effects of SDCs on Aβ1–42 fibrillation. WT K562 cells and SDC transfectants were incubated with Aβ1–42 at a concentration of 5 µM for 1 to 18 h at 37 °C. (a) After 1, 3, 6, and 18 h of incubation, the cells were treated with ThT at a concentration of 15 µM for 10 mins and fluorescence was measured. Amyloid fluorescence is expressed as fold change over background ThT fluorescence. The bars represent the mean ± SEM of four independent experiments. Statistical significance vs Aβ1–42-treated WT K562 cells was assessed by analysis of variance (ANOVA). *$p < 0.05$ vs Aβ1–42-treated WT K562 cells; **$p < 0.01$ vs Aβ1–42-treated WT K562 cells. (b) Scanning electron microscope visualization of WT K562 cells and SDC transfectants treated with Aβ1–42 at a concentration of 5 µM for 1, 6, or 18 h. Representative images of three independent experiments are shown. Scale bar = 1 µm. (c) CLSM visualization of ThT-labeled, intracellular Aβ1–42 fibrils in WT K562 cells and SDC transfectants. Representative images of three independent experiments are shown. Scale bar = 5 µm.

Confocal microscopy confirmed that SDCs promoted fibrillation and mediated intracellular translocation of Aβ1-42 oligomers. At 18 h, a significant increase in Aβ1-42 uptake was observed in all SDC transfectants compared to WT cells ($p < 0.01$). Among SDCs, SDC3 showed the highest uptake, while Trf internalization was reduced in all SDC transfectants, suggesting a distinct pathway for Aβ1-42 uptake. Colocalization assays indicated a substantial intracellular overlap between SDCs and Aβ1-42 with a high Mander's overlap coefficient (MOC > 0.7), confirming a common internalization pathway. The figure illustrates colocalization between SDCs and Aβ1-42, displaying fluorescent signals and high MOC values indicating strong colocalization (Figure 6).

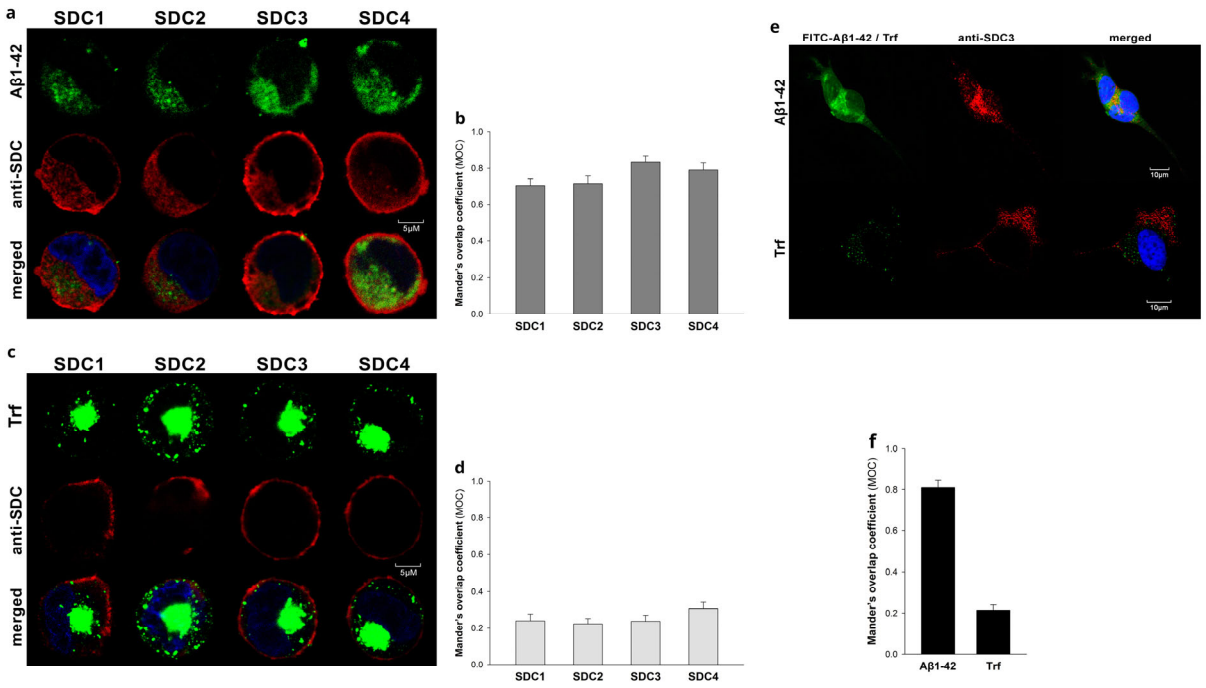

Figure 6. Colocalization of Aβ1–42 and SDCs. SDC transfectants or WT SH-SY5Y cells were treated with either FITC-Aβ1–42 or FITC-Trf for 18 h at 37 °C. After incubation, the cells were permeabilized and treated with the respective APC-labeled SDC antibody. The nuclei of cells were stained with DAPI, and cellular uptake was then analyzed using CLSM. (a,c) CLSM images of SDC transfectants treated with either FITC-Aβ1–42 (a) or FITC Trf (c) and respective APC-labeled SDC antibodies. Representative images of three independent experiments are shown. Scale bar = 5 µm. (b,d) Mander's overlap coefficient (MOC) ± SEM for the overlap of SDCs with FITC-Aβ1–42 (b) or FITC-Trf (d) was calculated by analysis of 21 images with ~7 cells in each image (from three separate samples). (e) CLSM images of WT SH-SY5Y cells treated with FITC-Aβ1–42 or FITC-Trf, along with APC-labeled SDC3 antibody. Representative images of three independent experiments are shown. Scale bar = 10 µm. (f) Mander's overlap coefficient (MOC) ± SEM for the overlap of SDC3 with FITC-Aβ1–42 or FITC-Trf was calculated by analysis of 21 images with ~7 cells in each image (from three separate samples)

In our study, we highlight the key role of SDC3 and SDC4 in Aβ1-42 uptake and fibrillation and the role of heparan sulfate chains and lipid pathways in the background of amyloid pathology. Flotillins, the membrane proteins that define lipid rafts, colocalize with SDCs and Aβ1-42 in intracellular compartments. Our confocal microscopy and proteomic studies confirmed that internalization of Aβ1-42 through SDCs occurs via flotillin-dependent lipid rafts, an alternative to clathrin- and caveolin-mediated endocytosis. Using sodium chlorate to inhibit the sulfation of SDC, we found that desulfation significantly reduced the binding of Aβ1-42, especially in SDC3 and SDC4 transfectants. Our scanning electron microscopy experiments confirmed that reduced sulfation inhibited Aβ1-42 fibril formation. Structural mutants of SDC4 were used to determine the contribution of specific extracellular domains. Mutants lacking heparan sulfate chains (pSi4 and CBD.pSi4) did not increase Aβ1-42 uptake, suggesting a crucial role for heparan sulfate chains in mediating this interaction. Mutants with truncated extracellular domains that retained the heparan sulfate chains (HSA.pSi4) showed increased Aβ1-42 uptake similar to WT SDC4 transfectants, confirming the importance of these chains in Aβ1-42 internalization (Figure 7).

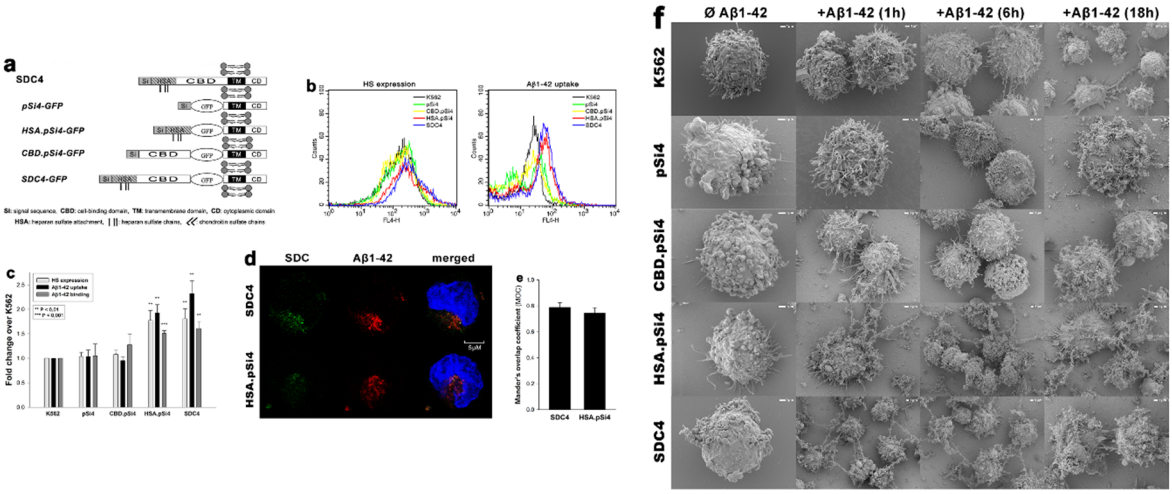

Figure 7. Contribution of various parts of the SDC4 ectodomain to Aβ1–42 uptake. WT K562 cells and SDC4mutants were treated with Aβ1–42 at a concentration of 5 µM at 37 °C. (a) Schematic representation of SDC4 deletion mutants used in the study. (b) Flow cytometry histograms representing HS expression and intracellular fluorescence of WT K562 cells and SDC4 mutants treated with FITC-Aβ1–42 for 18 h. (c) Results of flow cytometric measurements. As standards, fluorescence intensities are normalized to FITC-Aβ1–42-treated WT K562 cells. The bars represent the mean ± SEM of four independent experiments. Statistical significance vs. FITC-Aβ1–42-treated WT K562 cells was assessed by analysis of variance (ANOVA). **$p < 0.01$ vs standards; ***$p < 0.001$ vs standards. (d) CLSM visualization of SDC4 or HSA.pSi4 transfectants treated with FITC-Aβ1-42 for 18 h. Scale bar = 5 µm. (e) Mander's overlap coefficient (MOC) ± SEM for the overlap of Aβ1–42 with either SDC4 or HAS.pSi4 was calculated by analysis of 21 images with ~7 cells in each image (from three separate samples).

(f) Scanning electron microscope visualization of the cellular surface of Aβ1–42-treated WT K562 cells and SDC4 mutants. Representative images of three independent experiments are shown. Scale bar = 1 μm.

To highlight the crucial role of SDC3, we showed that overexpression of SDC3 in SH-SY5Y neuroblastoma cells enhanced cellular uptake and fibrillation of Aβ1-42. A significant correlation was found between SDC3 expression and Aβ1-42 uptake (r = 0.63) and fibrillation (r = 0.80), further confirming the critical role of SDCs, particularly SDC3, in mediating these processes in neuronal cells (Figure 8).

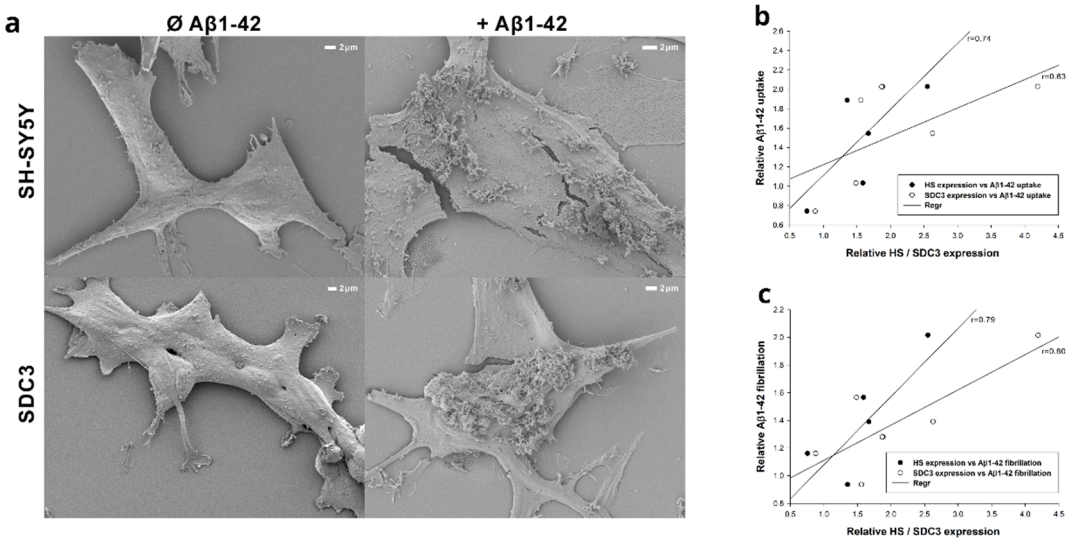

Figure 8. Effect of SDC3 on Aβ1–42 uptake and fibrillation in neurons. (a) Scanning electron microscopy visualization of Aβ1–42 attachment and fibrillation on WT SH-SY5Y cells and SDC3 mutants. Representative images of three independent experiments are shown. Scale bar = 2 μm. (b,c) Linear regression between HS or SDC3 expression and Aβ1–42 uptake or fibrillation.

We investigated the contribution of the syndecan (SDC) protein family to the cellular uptake, aggregation and spreading of α-syn and tau fibrils. Our results highlighted the essential role of SDCs, particularly SDC3, in promoting the internalization of misfolded proteins and their dependence on heparan sulfate (HS) chains and lipid raft pathways. The effects of different SDC isoforms on α-syn and tau fibril uptake were investigated using SDC-overexpressing K562 cells, a cell line with low levels of other heparan sulfate proteoglycans (HSPGs) and no detectable caveolin-1, which ensures minimal interference with other internalization pathways. Our results showed that SDC3, predominantly expressed in neurons, significantly enhanced cellular uptake of both α-syn and tau fibrils. In contrast, SDC4 did not considerably alter fibril uptake. Internalization of fibrils by SDC-transfected cells occurred via lipid raft-dependent but clathrin- and caveolin-independent pathways, as shown by flotillin colocalization assays (Figure 9).

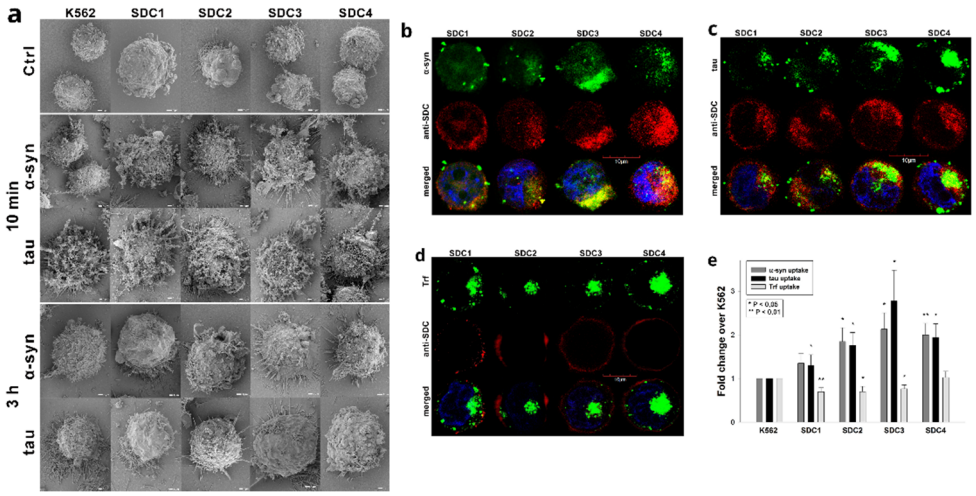

Figure 9. Cellular uptake of α-syn and tau fibrils into SDC transfectants. WT K562 cells and SDC transfectants were incubated with either of the FITC-labeled fibrils (α-syn or tau at a concentration of 5 μM monomer equivalent) or Trf (25 μg/ml) for 3h at 37°C. Cellular uptake of the fibrils and Trf was then analyzed with flow cytometry and microscopy. **(a)** Scanning electron microscope visualization of α-syn and tau fibrils, along with WT K562 cells and SDC transfectants treated with the fibrils at 10 min and 3 h of incubation. **(b-d)** CLSM visualization of fibril (α-syn, tau) and Trf uptake. (**b-d**) Colocalization of α-syn or tau fibrils and SDCs. SDC transfectants treated with either of the fluorescent fibrils (α-syn or tau) or Trf for 3 h were permeabilized and treated with the respective APC-labeled SDC antibody. The nuclei of cells were stained with DAPI, and cellular uptake was then analyzed using CLSM. Representative images of three independent experiments are shown. Scale bar = 10 μm. **(e)** Detected fluorescence intensities were normalized to fibril (α-syn or tau) or Trf-treated WT K562 cells as standards. The bars represent the mean ± SEM of five independent experiments. Statistical significance vs standards was assessed by analysis of variance (ANOVA). *p<0.05 vs standards; **p<0.01 vs standards.

We also investigated the role of heparan sulphate chains in fibril recruitment. To examine the role of heparan sulfate (HS) chains in mediating the interaction between SDCs and fibrils, sodium chlorate (NaClO3), an inhibitor of HS sulfation, was used. Treatment with NaClO3 significantly reduced the uptake of α-syn and tau fibrils, highlighting the essential role of polyanionic HS chains in these interactions. Further analysis of SDC4 mutants revealed that HS chains, rather than the cell-binding domain (CBD), are critical for fibril uptake. Mutants lacking HS chains, such as pSi4 and CBD.pSi4, did not show a significant increase in fibril uptake, whereas mutants containing only HS chains (HSA.pSi4) showed fibril internalization levels similar to wild-type SDC4 (Figure 10). This confirms HS chains' importance in mediating the cellular uptake of α-syn and tau fibrils.

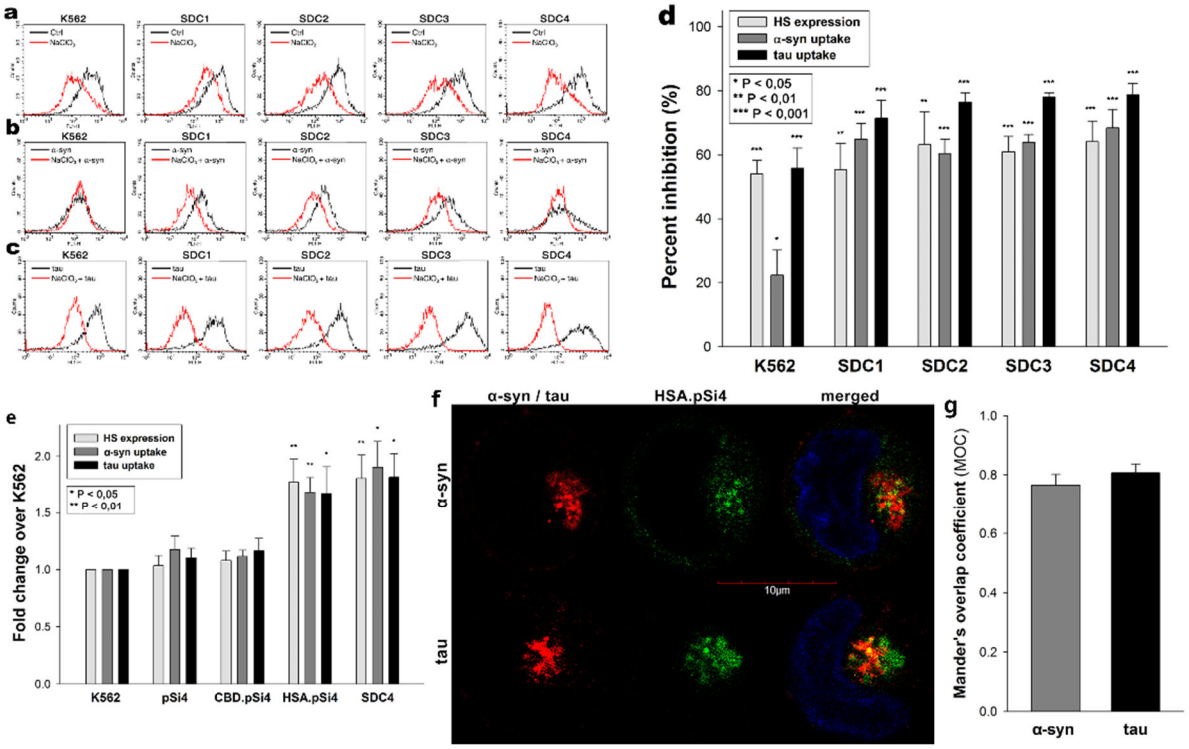

Figure 10. Effect of SDC domains on α-syn and tau fibril uptake. (a) Flow cytometry histograms representing HS expression of WT K562 cells or SDC transfectants after NaClO3 treatment. (b-c) Flow cytometry histograms representing intracellular fluorescence of fluorescent (FITC) fibril (α-syn or tau) treated WT K562 cells and SDC transfectants preincubated with or without NaClO3. (d) The effect of NaClO3 was expressed as percent inhibition, calculated with the following formula: $[(X - Y)/X] \times 100$, where X is the fluorescence intensity obtained on cells treated with either of the fibrils in the absence of NaClO3 and Y is the fluorescence intensity obtained on cells treated with either of the fibrils in the presence of NaClO3. The bars represent the mean ± SEM of four independent experiments. Statistical significance vs controls, untreated with NaClO3, was assessed by analysis of variance (ANOVA). *p<0.05 vs standards; **p<0.01 vs standards; ***p<0.001 vs standards. (e) Results of flow cytometric measurements. Detected fluorescence intensities were normalized to fibril-treated WT K562 cells as standards. The bars represent the mean ± SEM of four independent experiments. Statistical significance vs fibril-treated WT K562 cells (standards) was assessed by analysis of variance (ANOVA). *p<0.05 vs standards; **p<0.01 vs standards. (f) CLSM visualization of HSA.pSi4 transfectants treated with fluorescent α-syn and tau fibrils for 3h. Scale bar = 5 µm. (g) MOC ± SEM for the overlap of fluorescent α-syn and tau fibrils with HSA.pSi4 was calculated by analyzing 21 cellular images (7 images per sample, experiments performed in triplicate).

We further explored how SDCs influence the conformation of α-syn and tau by incubating monomeric α-syn and tau with SDC-transfected K562 cells. This experiment revealed that SDC3 (and, to a lesser extent, SDC4) promoted the fibrillation of both proteins over time (Figure 11). Scanning electron microscopy (SEM) showed an increased number of mature fibrils on the cell surface of SDC-transfected cells after 18 hours of incubation, further supporting the notion that SDCs trigger the fibrillation of α-syn and tau. Importantly, when

fibrillation occurred, the SDC-mediated uptake of fibrils was significantly higher, suggesting that once fibrils were formed, SDCs facilitated their internalization.

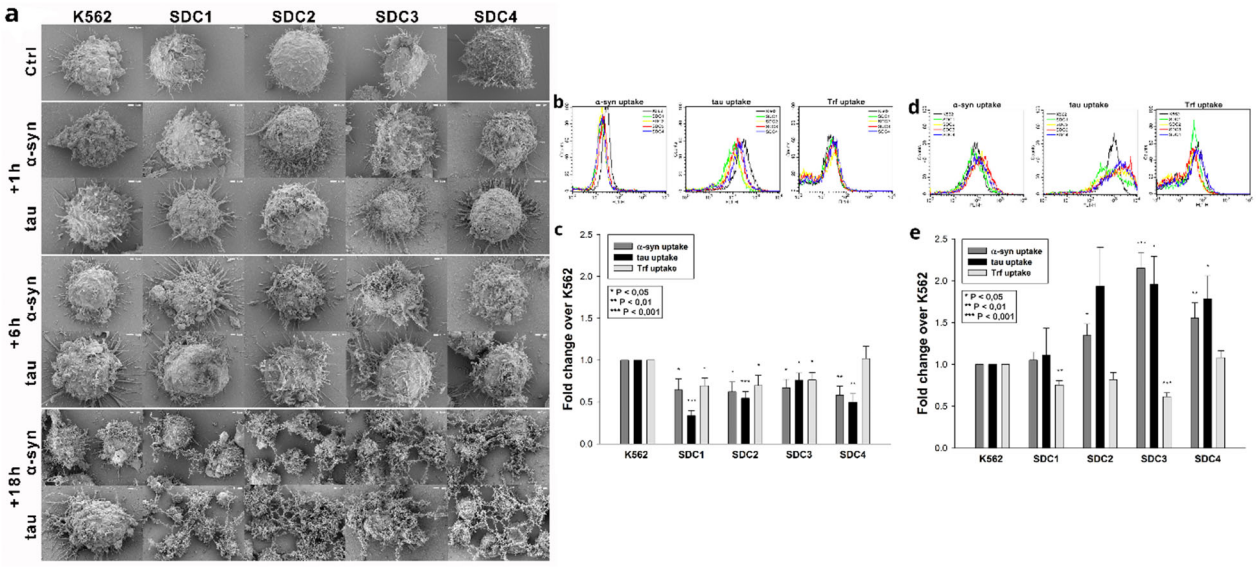

Figure 11. Effects of SDCs on α-syn and tau fibrillation. WT K562 cells and SDC transfectants were incubated with α-syn and tau monomers at a concentration of 5 μM for up to 18 h at 37 °C. (a) Scanning electron microscope visualization of the cellular surface of WT K562 cells and SDC transfectants treated with α-syn or tau monomers for 1h, 6h, and 18h. Representative images of three independent experiments are shown. Scale bar = 1 μm. Cellular uptake of α-syn and tau into WT K562 cells and SDC transfectants following treatment with the monomers. WT K562 cells and SDC transfectants were treated with monomeric, FITC-labeled, or unlabeled α-syn, tau at a concentration of 5 μM or Trf (25 μg/ml) for 1 or 18 h at 37 °C. (b,d) Flow cytometry histograms showing intracellular fluorescence following 1 (b) or 18 h (d) incubation with either of the proteins (α-syn, tau, or Trf). (c,e) Results of flow cytometric measurements. Detected fluorescence intensities are normalized to WT K562 cells treated with the respective fluorescent proteins (standards). The bars represent the mean ± SEM of five independent experiments. Statistical significance vs protein-treated (either α-syn, tau or Trf) WT K562 cells (standards) was assessed by analysis of variance (ANOVA). **p<0.01 vs standards; ***p<0.001 vs standards.

To assess the role of SDC3 in a more physiologically relevant neuronal context, we studied its effect on fibril uptake in SH-SY5Y cells—a human neuroblastoma cell line. Overexpression of SDC3 in both differentiated and undifferentiated SH-SY5Y cells led to increased fibril uptake, especially after 18 hours, when fibrils had already formed. Colocalization studies confirmed the intracellular colocalization of SDC3 with α-syn and tau fibrils, supporting the notion that SDC3 mediates fibril uptake in a lipid raft-dependent manner (Figure 12).

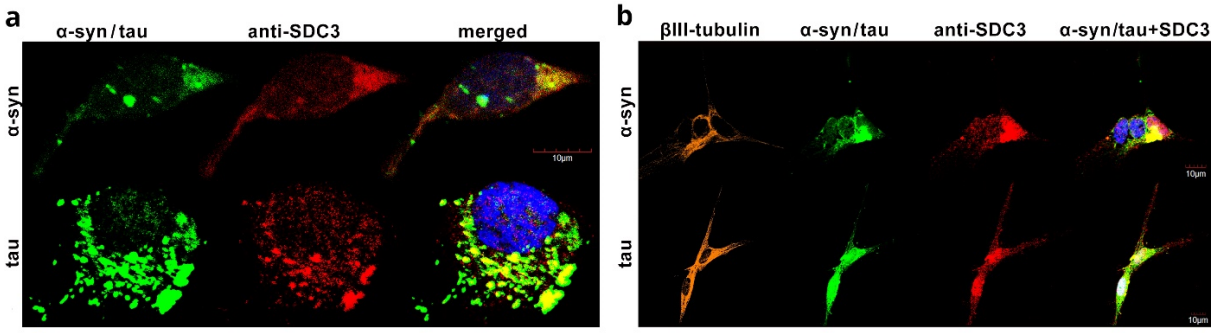

Figure 12. Effect of SDC3 overexpression on α−syn and tau fibril uptake in SH-SY5Y cells. Colocalization of the fibrils with SDC3 in undifferentiated (a) or differentiated (b) SH-SY5Y cells. CLSM images of WT SH-SY5Y cells treated with either of the FITC-labeled fibrils (α−syn or tau), along with APC-labeled SDC3 antibody. In the case of differentiated SH-SY5Y cells (DIF), neuronal differentiation was justified by staining the cells with neuron-specific human βIII-tubulin antibody and Alexa Fluor 546-labeled secondary antibody. Scale bar = 10 μm.

Additionally, Co-IP experiments confirmed that flotillin-1 and flotillin-2, markers of lipid rafts, co-immunoprecipitated with SDC3 and α-syn/tau fibrils, further confirming the role of lipid rafts in this process (Figure 13).

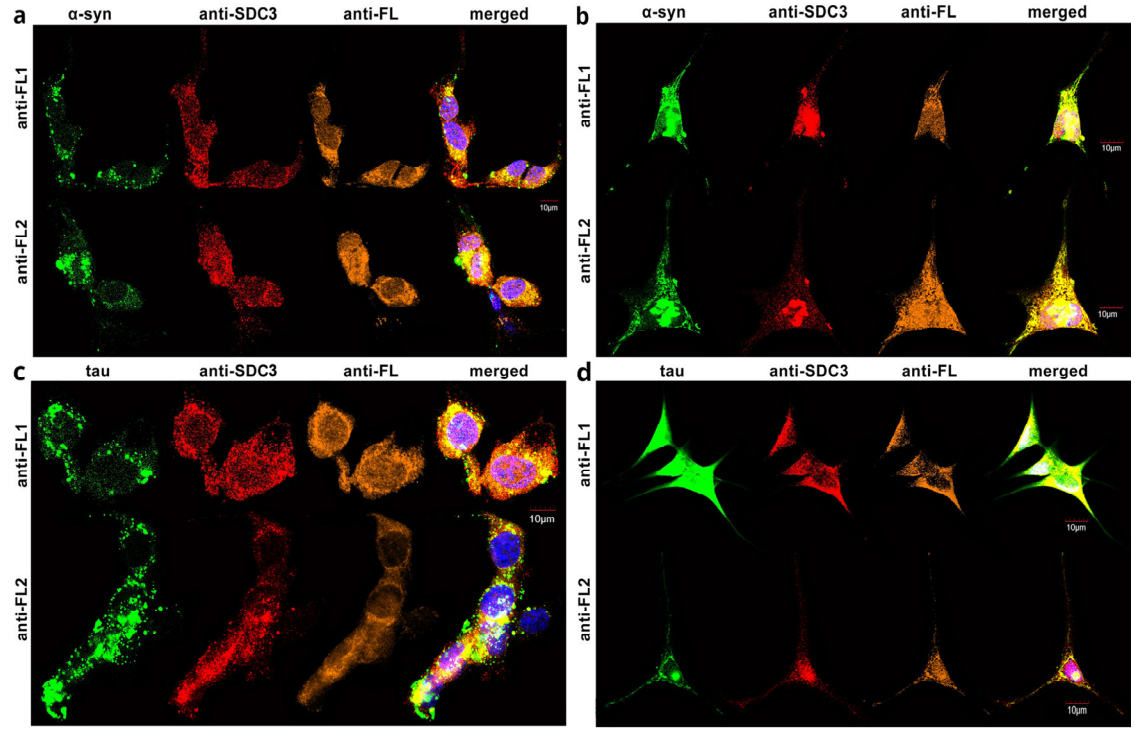

Figure 13. Colocalization of the fibrils with flotillins in undifferentiated (a,c) or differentiated (b,d) SH-SY5Y cells. CLSM images of WT SH-SY5Y cells treated with either of the fluorescent fibrils (α−syn or tau), along with APC-labeled SDC3 antibody and either of the Alexa Fluor 546-labeled FLOT1 and FLOT2 antibodies. Scale bar = 10 μm.

Finally, we investigated the conformation-dependent nature of SDC-mediated uptake. We found that monomeric α-syn and tau were taken up at lower levels than the fibrillar forms, with significant uptake occurring only after fibrillation, especially in SDC-overexpressing cells. Confocal microscopy revealed that SDC3 significantly facilitated the internalization of fibrillar α-syn and tau but not the monomeric forms (Figure 14). These findings suggest that the fibrillar form of the proteins primarily triggers SDC-mediated internalization.

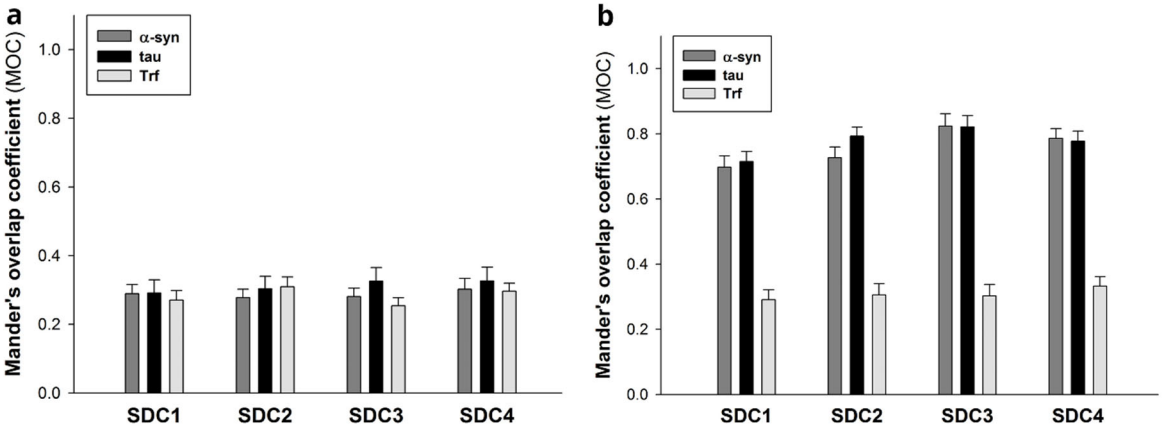

Figure 14. Colocalization studies after treatment with the monomers. SDC transfectants (established in K562 cells) were treated with either of the fluorescently labeled α−syn, tau monomers (at a concentration of 5 μM) or Trf (25 μg/ml) for 1 h or 18 h at 37 °C. After incubation, the cells were permeabilized and treated with the respective APC-labeled SDC antibody. The nuclei of cells were stained with DAPI, and cellular uptake was then analyzed using CLSM. (a) Mander's overlap coefficient (MOC) ± SEM for the overlap of SDCs with either of the fluorescently labeled monomer proteins (α−syn, tau) and Trf was calculated by analyzing 21 cellular images (7 images per sample, experiments performed in triplicate). (b) MOC ± SEM for the overlap of SDCs with either of the fluorescently labeled monomer proteins (α−syn, tau) and Trf was calculated by analyzing 21 cellular images (7 images per sample, experiments performed in triplicate).

SDCs increase the cellular internalization of ApoE isoforms; therefore, the cellular uptake of ApoE isoforms was investigated using SDC-specific cell models [19,53,89]. The poor HSPG expression of K562 cells and their inability to form caveolae, the source of caveolar endocytosis, make K562 cells an ideal cell line to study the effect of overexpression of SDCs on ApoE uptake while avoiding the confounding effects of endocytosis mediated by other HSPGs or caveolae [19,24]. Since the role of HS chains in ApoE binding has been evaluated [100-102]. Therefore, SDC transfectants with nearly identical HS expression were selected and treated with FITC-tagged ApoE isoforms (ApoE2, 3, and 4) and WT K562 cells. (It should be noted that SDC overexpression did not affect LRP1 expression. Thus, LRP1 expression in SDC-

transfectants was identical to that in WT K562 cells. After 3 h of incubation with FITC-labeled ApoEs, the cells were washed, and ApoE uptake was quantified with flow cytometry [83]. The internalization of ApoE isoforms was measured by adding trypan blue (dissolved at a concentration of 0.25% in ice-cold 0.1 M citrate buffer) 1 min before the flow cytometric analyses; hence, the fluorescence of extracellularly attached ApoE isoforms was quenched [19,53,83]. Our flow cytometry studies of ApoE-treated SDC transfectants showed that SDC overexpression increased cellular uptake of ApoE in an isoform-dependent manner. Among SDCs, neuronal SDC3 increased ApoE internalization the most (Figure 15).

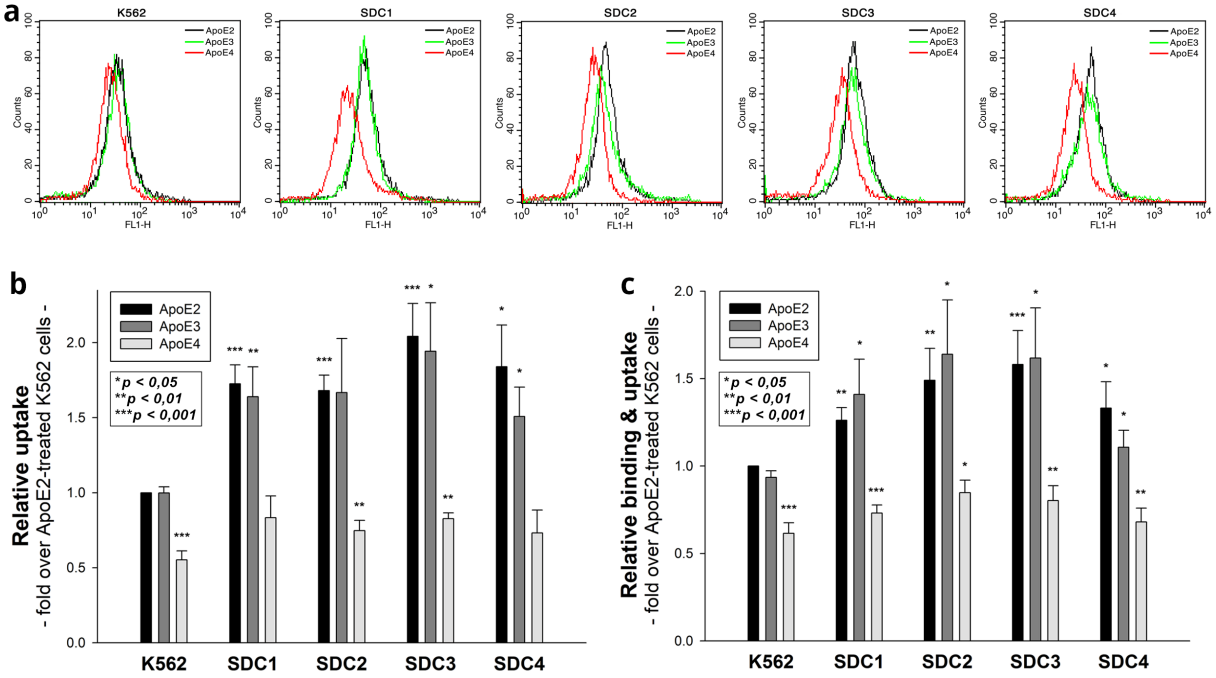

Figure 15. Cellular uptake of ApoEs into WT K562 cells and SDC transfectants. WT K562 cells and SDC transfectants were treated with either of the FITC-labeled ApoE isoforms for 3 h at 37 °C. Cellular uptake of ApoE isoforms was then measured with flow cytometry and confocal microscopy. (a) Flow cytometry histograms representing intracellular fluorescence of WT K562 cells and SDC transfectants treated with FITC-labeled ApoEs. (b,c) As standards, detected intracellular and cellular fluorescence intensities were normalized to FITC-ApoE2-treated WT K562 cells. The bars represent the mean ± SEM of six independent experiments. Statistical significance vs. standards (i.e., FITC-ApoE2-treated WT K562 cells) was assessed with analysis of variance (ANOVA). * $p < 0.05$; ** $p < 0.01$; *** $p < 0.001$.

Among ApoEs, SDCs increased ApoE2 and ApoE3 uptake most effectively, while SDCs' effect on increasing ApoE4 uptake was lower [83]. Compared to ApoE-treated WT K562 cells, the overall cellular fluorescence of FITC-ApoE-treated SDC transfectants also increased, indicating that SDC overexpression increased both the cellular binding and the uptake of ApoE

[83]. Our colocalization assays also showed that SDC3 and SDC4 showed the strongest interaction with ApoE2 and ApoE3, as measured by Mander's overlap coefficient (MOC) and Pearson's correlation coefficient (PCC), respectively (Figure 16). Utilizing the Mander's overlap coefficient (MOC, showing the percentage of pixels overlapped on a scale of 0 to 1 to measure the degree of overlap between ApoEs and SDCs, our colocalization studies showed that approximately half of ApoEs overlap with SDC3 or SDC4 (i.e., MOC ~0.50) [83,103,104]. However, the MOCs for SDC1 and ApoEs were slightly lower (MOC ~0.40). Based on the MOC values detected, the overlap between all ApoEs and SDC2 was the lowest. To reveal a more detailed picture of colocalization, we also analyzed the correlation between ApoEs and SDCs using Pearson's correlation coefficient (PCC) [105]. The observed PCC values between ApoEs and SDC3 and 4 showed a moderate correlation (i.e., PCC ~0.4), while PCC values between ApoEs and SDC1 were slightly lower (i.e., PCC ~0.3). Similar to MOC, PCC values of ApoEs with SDC2 were the lowest, indicating a low correlation.

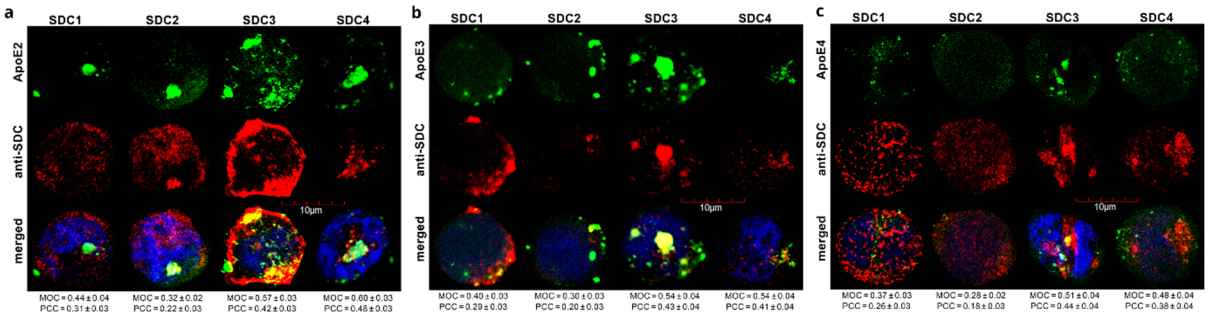

Figure 16. Colocalization of ApoEs and SDCs. SDC transfectants were treated with either of the FITC-ApoEs for 3 h at 37 °C. After incubation, the cells were permeabilized and treated with the respective APC-labeled SDC antibody. The nuclei of cells were stained with DAPI, and colocalization was then analyzed using confocal microscopy. (a–c) Confocal microscopic images of SDC transfectants treated either of the FITC-ApoEs and the respective APC-labeled SDC antibody. Representative images of three independent experiments are shown. Scale bar = 10 µm. MOC or PCC ± SEM for the colocalization of SDCs with FITC-ApoEs was calculated by analyzing 18 images with ~7 cells in each image (from three separate samples).

In immunoprecipitation of SDC3-treated extracts from SDC3-treated SDC3 transfectants with ApoE, ApoE2 showed the strongest band, followed by ApoE3 and 4, confirming the previously observed differences in internalization efficiency of ApoE isoforms (ApoE2 ≥ ApoE3 > ApoE4).

After assessing the contribution of SDCs to the cellular uptake of ApoE isoforms in a cellular model with a reasonably low HSPG expression, we advanced to studies on SH-SY5Y cells, a widely used in vitro model of neuronal cell lines [83,90,106,107]. Our microscopic colocalization

assays on undifferentiated and differentiated SH-SY5Y cells gave a MOC of ~0.5 between SDC3 and ApoE2 or ApoE3, indicating that approximately half of ApoE2 and ApoE3 colocalize with SDC3 during internalization. The MOC value was slightly lower for SDC3 and ApoE4. Quantification of colocalization with PCC showed a value of ~0.4 for ApoE2/3 and SDC3 and ~0.3 for ApoE4 and SDC3, indicating moderate colocalization. Following immunoprecipitation of SDC3 from extracts of ApoE-treated differentiated SH-SY5Y cells, ApoE2 showed the strongest band, followed by ApoE3 and 4, further confirming the differences previously identified in the internalization efficiency of ApoE isoforms (Figure 17).

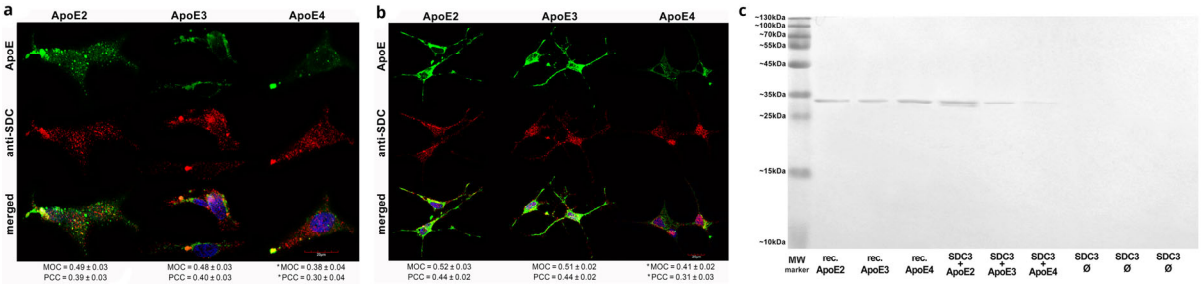

Figure 17. Colocalization of ApoEs with SDC3 in SH-SY5Y cells. (a,b) Undifferentiated (a) or differentiated (b) SH-SY5Y cells were treated with either of the FITC-ApoEs for 3 h at 37 °C. After incubation, the cells were permeabilized and treated with the APC-labeled SDC3 antibody. The nuclei of cells were stained with DAPI, and colocalization was then analyzed using confocal microscopy. Representative images of three independent experiments are shown. Scale bar = 20 µm. MOC and PCC ± SEM, for the colocalization of SDCs with FITC-ApoEs, was calculated by analyzing 21 images with ~7 cells in each image (from three separate samples). (c) SDS-PAGE showing FITC-labeled ApoEs immunoprecipitated with SDC3 from extracts of differentiated SH-SY5Y. Lane 1: MW marker. Lanes 2–4: 0.5 µg of FITC-ApoE2,3 and 4, respectively. Lanes 5–7: immunoprecipitate of SH-SY5Y cells treated with either of the FITC-ApoEs. Lanes 8–10: immunoprecipitate of untreated SH-SY5Y cells. Standard protein size markers are indicated on the left. Image acquisition was carried out with the UVITEC Alliance Q9 Advanced Imager.

Overexpressing SDC3 in differentiated SH-SY5Y cells increased uptake for all ApoE isoforms. Among ApoEs, ApoE2 exhibited the highest internalization efficacy, while ApoE4 exhibited the lowest. The extent of the increase in ApoE uptake was similar to the rise in SDC3 expression (Figure 18).

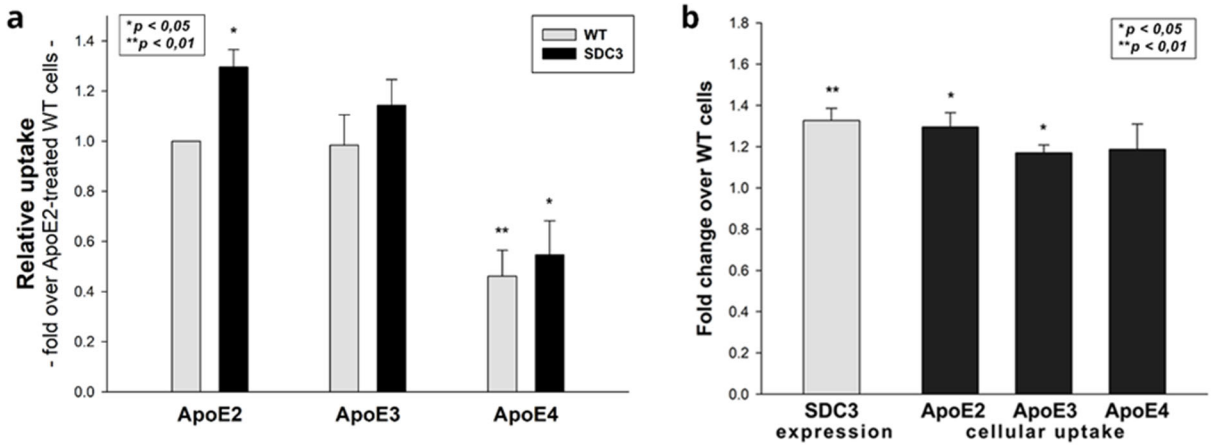

Figure 18. SDC3 overexpression increases ApoE uptake into SH-SY5Y cells. SDC3-overexpressing clones created in differentiated SH-SY5Y cells were selected by measuring SDC3 expression with flow cytometry. (a) Detected intracellular fluorescence intensities were normalized to FITC-ApoE2-treated WT SH-SY5Y cells as standards. The bars represent the mean ± SEM of three independent experiments. Statistical significance vs. standards was assessed with ANOVA. (b) Fold change in SDC3 expression, along with ApoE uptake following SDC3 overexpression in differentiated SH-SY5Y cells. The bars represent the mean ± SEM of three independent experiments. The statistical significance vs. ApoE2-treated WT SH-SY5Y cells as standards was assessed with ANOVA. * $p < 0.05$; ** $p < 0.01$.

To investigate the effect on amyloid pathology, we looked at the impact of ApoEs on the aggregation of amyloid beta (Aβ1-42) in SDC3-overexpressing SH-SY5Y cells. The SDC3 overexpression increased the fibrillation of Aβ1–42 at 18 h, while its effect at 3 h of incubation was insignificant. ApoEs exerted differential effects on Aβ1–42 aggregation: ApoE2 decreased Aβ1–42 aggregation, even in SDC3-overexpressing transfectants at 18 h, while ApoE4 markedly increased it, both in the case of the WT SH-SY5Y cells and the SDC3 transfectants [83]. Scanning electron microscopy confirmed these results, with ApoE2 reducing and ApoE4 increasing the number of aggregates. These effects of ApoE2 and 4 were instead striking on SDC3-overexpressing SH-SY5Y cells [83]. Furthermore, ApoE isoforms affected the uptake of Aβ1-42, with ApoE2 increasing uptake within 3 h, while ApoE4 had the opposite effect within 18 h, increasing the internalization of Aβ1-42 (Figure 19).

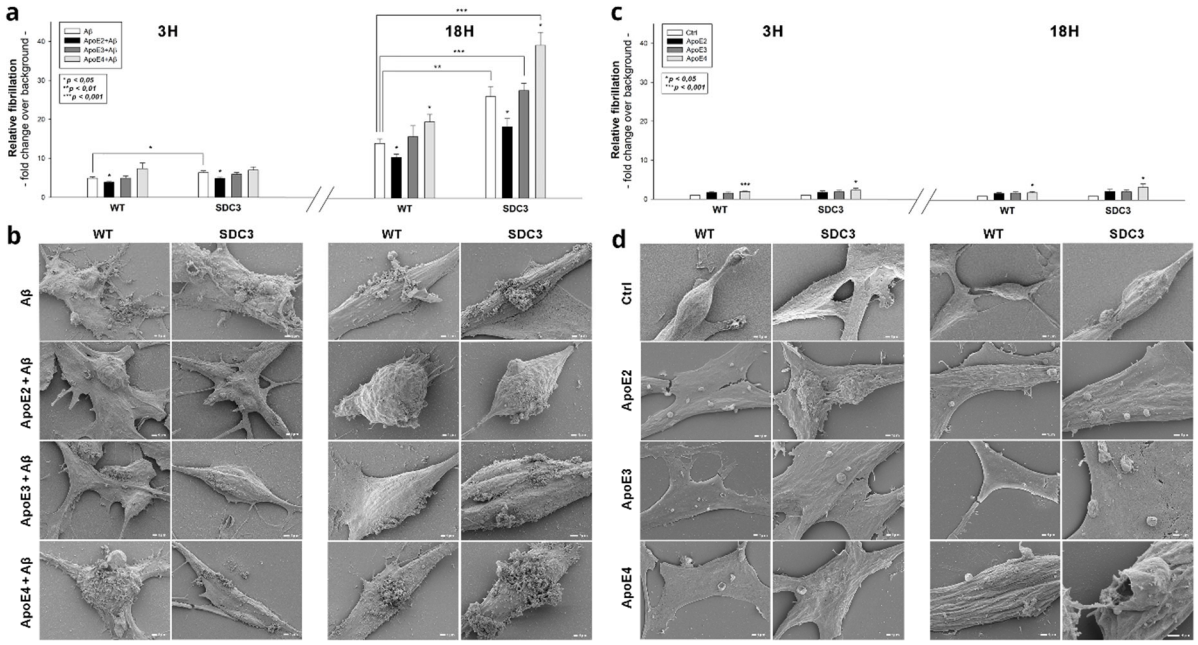

Figure 19. The effect of ApoEs on Aβ1-42 fibrillation in WT and SDC3-overexpressing differentiated SH-SY5Y cells. WT and SDC3-overexpressing differentiated SH-SY5Y cells were incubated with either of the ApoE isoforms at 37 °C. Thirty minutes later, some of the cells were treated with Aβ1–42 and incubated for either 3 h or 18 h (a,b). After incubation, fibrillation was analyzed with either ThT staining or electron microscopy. (a,c) Results of ThT fluorescence assays after 3 h and 18 h of incubation with Aβ1–42 in the presence or absence of ApoEs (a) or the ApoE isoforms alone (c). Amyloid fluorescence is expressed as fold change over background ThT fluorescence. The bars represent the mean ± SEM of four independent experiments. In the case of Aβ1–42 treatment (a), statistical significance was assessed vs. Aβ1–42-only treated cells with ANOVA. Statistical significance was assessed for cells receiving ApoE treatment only (b) vs. untreated controls. * $p < 0.05$; ** $p < 0.01$; *** $p < 0.001$. (b,d) Scanning electron microscope visualization of WT and SDC3-overexpressing differentiated SH-SY5Y cells at 3 h and 18 h of incubation with Aβ1–42 in the presence or absence of ApoEs (b) or the ApoE isoforms alone (d). Representative images of three independent experiments are shown. Scale bar = 1 μm.

Recent studies have explored small regions with amyloidogenic properties in the amino acid sequences of ApoE3 and 4, showing that these aggregation hot spots would drive the self-assembly of amyloid-like fibrils [83,108]. Thus, we also examined the fibrillation of ApoEs isoforms in the absence of Aβ1–42. The fluorescence studies on ApoE-treated SH-SY5Y cells and SDC3 transfectants revealed the fibrillation of ApoE4 at both 3 and 18 h of incubation (along with the fibrillation of ApoE3 at 3 h (Fig. 19c). Compared to Aβ1–42 (Fig. 19b), the extent of fibrillation of ApoE4 was less profound, as shown by the lower ThT fluorescence values obtained on ApoE-treated cells. Electron microscopic studies also show the formation of fibrillar-like aggregates on the surfaces of ApoE4-treated cells, especially at 18 h of incubation [83]. Such small fibrils on ApoE3-treated cells were less evident, while electron

microscopy did not reveal ApoE2 fibrils on ApoE2-treated SH-SY5Y cells and SDC3 transfectants (Fig. 19d).

Utilizing WT and SDC3-overexpressing differentiated SH-SY5Y cells, and we also explored the effect of ApoEs on Aβ1–42 uptake. In line with our previous findings, SDC3 overexpression increased the cellular uptake of Aβ1–42 at both 3 and 18 h of incubation [19]. ApoEs exerted various effects on Aβ1–42 uptake: at 3 h ApoE2 increased Aβ1–42 internalization, while ApoE4 reduced it (Fig. 20a). This effect of ApoEs on Aβ1–42 uptake was reversed at 18 h of incubation: ApoE4 increased Aβ1–42 uptake, while ApoE2 and 3 reduced it (Fig. 20d).

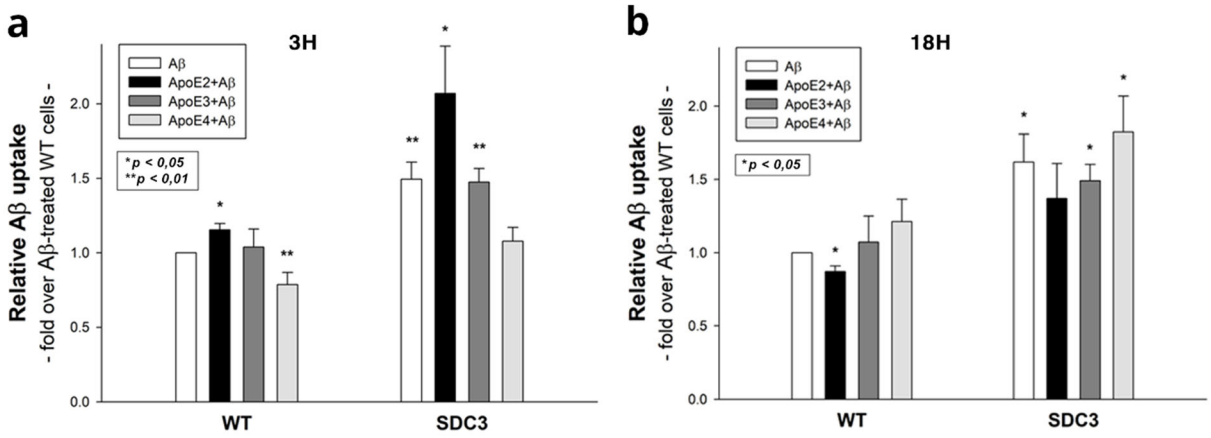

Figure 20. The effects of ApoEs on Aβ1–42 uptake in WT and SDC3-overexpressing differentiated SH-SY5Y cells. WT and SDC3-overexpressing differentiated SH-SY5Y cells were preincubated with different ApoEs for 30 min at 37 °C. The cells were then treated with FITC-labeled or, in the case of fibrillation studies, unlabeled Aβ1–42 for either 3 or 18 h. After incubation, the cellular uptake of Aβ1–42 was analyzed. (a,b) Detected intracellular fluorescence intensities were normalized to FITC-Aβ1–42-only treated WT SH-SY5Y cells as standards. The bars represent the mean ± SEM of four independent experiments. Statistical significance vs. standards was assessed with ANOVA. * $p < 0.05$; ** $p < 0.01$.

Confocal microscopy also showed an increased presence of ThT-labeled aggregates at 18 h in WT and SDC3-overexpressing differentiated SH-SY5Y cells, which was reduced in the case of samples pretreated with ApoE2. ApoE4, on the other hand, increased the number of ThT-labeled aggregates, indicating the increased presence of Aβ1–42 aggregates (Figure 21) [83].

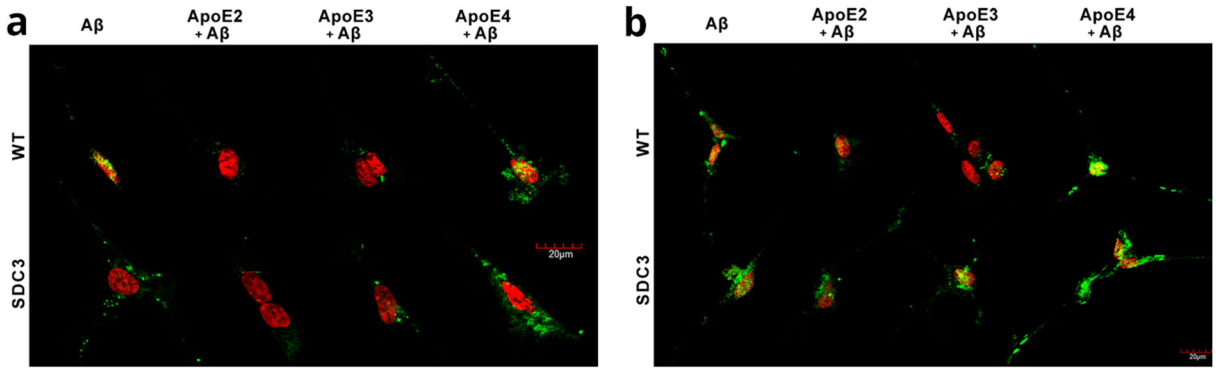

Figure 21. The effects of ApoEs on Aβ1–42 uptake in WT and SDC3-overexpressing differentiated SH-SY5Y cells. (a,b) Confocal microscopic visualization of ThT-labeled Aβ1–42 fibrils in WT and SDC3-overexpressing differentiated SH-SY5Y cells at 3 h (a) and 18 h (b) of incubation. The nuclei of cells were stained with DRAQ5. Representative images of three independent experiments are shown. Scale bar = 20 μm.

Confocal microscopy studies revealed that about half of the Congo Red-stained Aβ1–42 fibrils and ApoE4s overlap (i.e., MOC = 0.51 and PCC = 0.45), confirming previous findings on the colocalization of amyloid plaques and ApoE4 [86,109,110].

This result also shows that overexpression of SDC, particularly SDC3, enhances cellular uptake of ApoE isoforms in a cell type- and isoform-specific manner [83]. In addition, differential modulation of Aβ1-42 aggregation and uptake by ApoE isoforms provides new insights into the role of ApoE in amyloid pathology [83]. These results underscore the potential therapeutic relevance of targeting SDC3 to modulate ApoE-mediated cellular processes in neurodegenerative diseases.

The development of early diagnostics against AD is a key to detecting the disease in the stage of reasonably mild central nervous system (CNS) degeneration [12,111].

The role of SDC3 on endothelial cells is emerging in inflammatory responses [12,112]. SDC3 expressed on inflamed vascular endothelia binds leukocytes and chemokines during the progression of rheumatoid arthritis [113,114]. In the brain, endothelial cell SDCs also modulate the transendothelial migration of monocytes, thus contributing to the development of neuroinflammatory lesions [115]. Our study highlights that SDC3 plays a key role in neuroinflammation and neurodegeneration in Alzheimer's disease and can be used as a blood-based biomarker for diagnosing and monitoring the disease. Considering the scientific evidence on the importance of TNF-α in AD, we decided to analyze the effect of TNF-α on SDC3 expression of model cell lines representing two essential classes of cells in AD [12,116]. SH-SY5Y represents neuronal-like cells widely used in neurobiology, while hCMEC/D3 is a gold

standard cell line to study blood-brain barrier-derived endothelial cells [12,90,117]. Both cell lines have endogenous SDC3 expression and incubating them with TNF-α for seven days increased their SDC3 expression. The two cell lines significantly increased SDC3 overexpression due to TNF-α (Figure 22) [12].

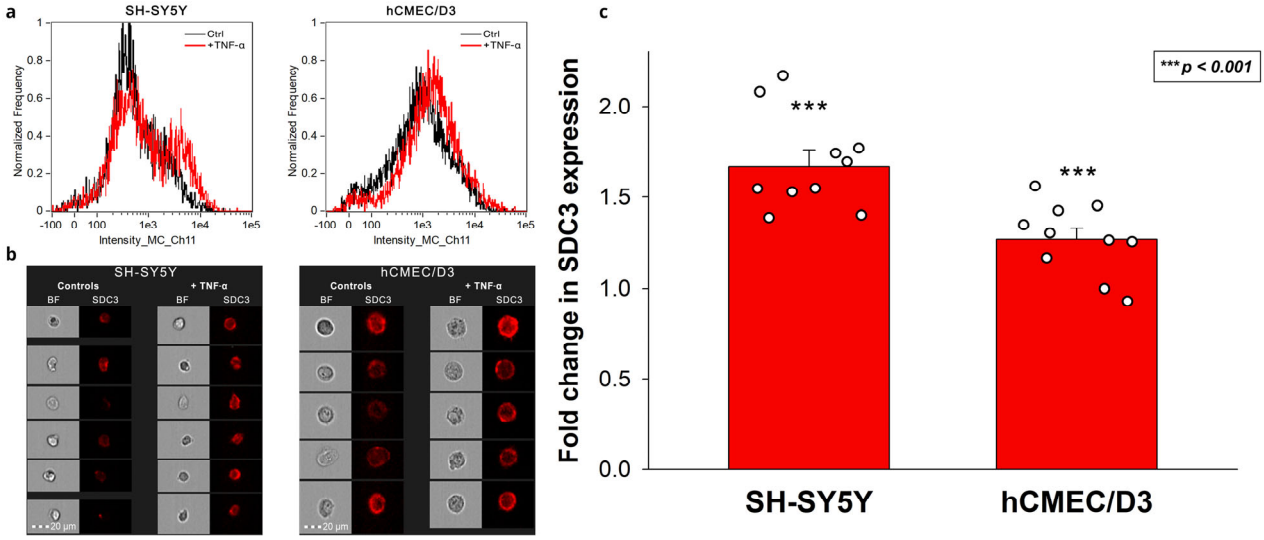

Figure 22. SDC3 expression of TNF-α-treated SH-SY5Y and hCMEC/D3 cells. Cells were incubated with or without (i.e., controls) 5 ng/mL TNF-α for 7 days. After incubation, the cells were treated with APC-labeled SDC3 antibody, and SDC3 was measured with imaging flow cytometry. (a) Representative flow cytometry histograms showing the SDC3 expression of SH-SY5Y and hCMEC/D3 cells. (b) Brightfield (BF) and fluorescent cellular images of SH-SY5Y and hCMEC/D3 cells treated with APC-labeled SDC3 antibody. Scale bar = 20 µm. (C) Detected fluorescence intensities were normalized to control cells untreated with TNF-α. The bars represent the mean + SEM of ten independent experiments. Statistical significance vs. controls was assessed with ANOVA. *** $p < 0.001$.

APPSWE-Tau is a double mutant transgenic mice model that develops neurofibrillary tangles and progressive motor disturbance and expresses mutant beta-amyloid precursor protein (APP), thus modulating the APP-Aβ environment [118]. In our studies, 12-month-old APPSWE-Tau mice, compared with wild-type (WT) C57BL/6 mice, exhibited significantly increased amyloid plaque load (Figure 23) [12].

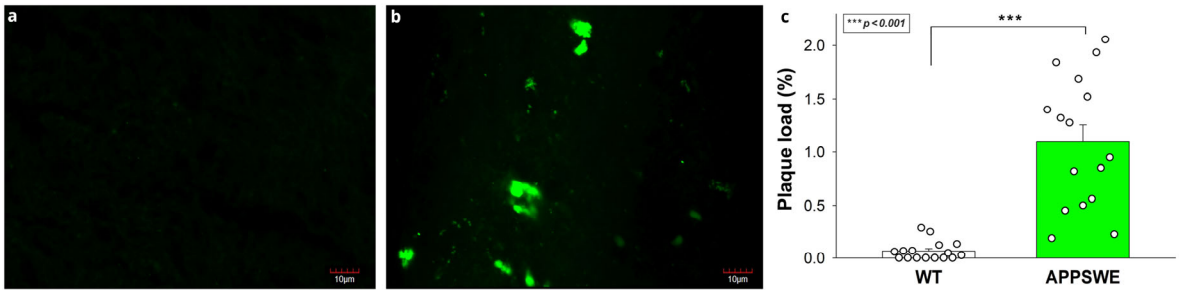

Figure 23. APPSWE-Tau mice exhibit significantly increased amyloid plaque load. (a,b) Representative brain slices WT (a) and APPSWE-Tau mice (b) stained with Aβ1-42 antibody. Scale bar = 100 µm. (c) The amyloid plaque load was quantified on Aβ1-42 antibody–stained frontal brain slices from 12-month-old APPSWE-Tau and WT mice. Each group contained 8 animals; the plaque load was measured in two slices of each animal. Data are expressed as mean + SEM. *** $p < 0.001$.

Increased Aβ plaque load was also associated with elevated TNF-α concentrations in APPSWE-Tau mice's brain samples, as shown by ELISA measurements. TNF-α blood concentrations of APPSWE-Tau were also significantly higher than those of WT controls. TNF-α concentration in the blood and the brain strongly correlated with a covariance of 0.80 (Figure 24).

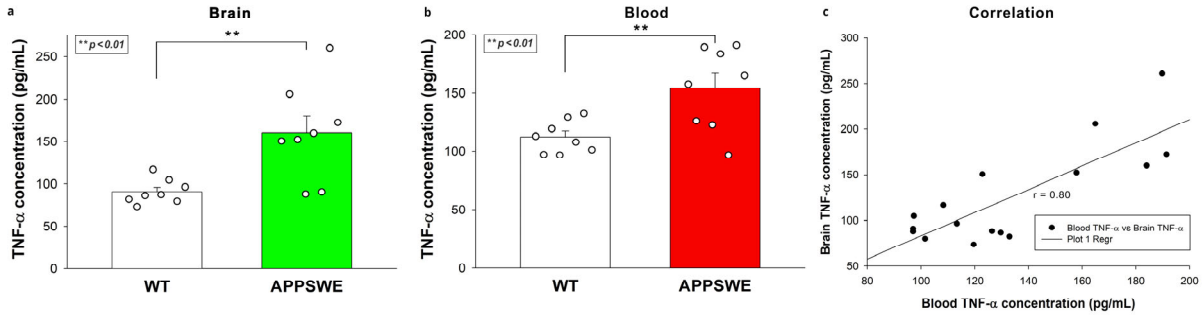

Figure 24. APPSWE-Tau mice exhibit increased TNF-α concentrations in the brain and the blood. (a,b) TNF-α concentrations of brain extracts (a) and whole blood (b) of APPSWE-Tau mice, along with representative WT controls, were measured with a mouse SDC3 ELISA kit. Each group contained 8 animals. The bars represent the mean + SEM. Statistical significance vs. WT was assessed with ANOVA. ** $p < 0.01$. (c) Linear regression between the TNF-α content of blood and brain.

Our ELISA measurements also showed increased SDC3 concentrations in the brain and the periphery, namely the liver. Increased SDC3 concentrations in the brain and liver correlated well with blood TNF-α concentrations, suggesting a causal relationship between TNF-α and SDC3 expression, as shown in previous in vitro studies.

Considering the emerging role of endothelial cells' SDC3 in the inflammatory response, along with our initial in vitro data on TNF-α-induced SDC3 expression in human blood-brain barrier (BBB) endothelial cells, we also analyzed the SDC3 expression of primary BBB endothelial

cells isolated from mice. Primary brain endothelial cells (PBECs) were isolated using the method of Assmann et al., and SDC3 expression was analyzed using imaging flow cytometry using fluorescent SDC3 antibodies [12,95]. A fluorescently labeled PECAM-1 (platelet endothelial cell adhesion molecule-1) antibody was used as an endothelial marker to identify PBECs during the flow cytometry analyses [12,119]. The SDC3 expression of PBECs isolated from APPSWE-Tau was significantly increased compared to those isolated from WT mice.

The roles of SDC3 on leukocytes are emerging in inflammatory responses [112]. TNF-α induces the SDC3 expression of cultured monocytes [12]. Considering the role of monocytes in AD progression, we also analyzed the SDC3 expression of monocytes isolated from the blood of APPSWE-Tau and WT mice. Thus, blood-derived monocytes were isolated with EasySep™ Mouse Monocyte Isolation Kit, stained with CD11b monocyte marker, and the SDC3 expression of CD11b positive cells was measured with imaging flow cytometry (Figure 25) [12,120]. Monocytes isolated from APPSWE-Tau mice exhibited increased SDC3 expression than those from WT mice [12]. SDC3 expression of blood-derived monocytes showed a positive correlation ($r = 0.81$) with Aβ plaque deposition in the brain, showing that SDC3 on monocytes is a good indicator of amyloid pathology in the brain [12].

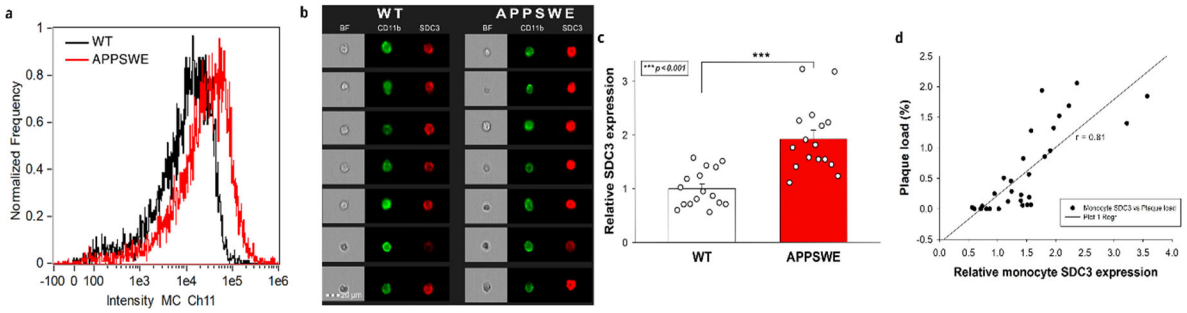

Figure 25. Monocytes isolated from APPSWE-Tau mice exhibit increased SDC3 expression. Isolated monocytes were treated with CD11b and SDC3 antibodies, and SDC3 expression of CD11b positive cells was analyzed with imaging flow cytometry. (a) Representative histogram showing the SDC3 expression of monocytes isolated from APPSWE-Tau and WT mice. (b) BF and fluorescent cellular images of CD11b and SDC3 antibody-treated monocytes isolated from APPSWE-Tau and WT mice. Each group contained eight animals. SDC3 expression of each sample was measured twice. (c) Detected fluorescence intensities were normalized to WT. The bars represent the mean + SEM. Statistical significance vs. WT was assessed with ANOVA. *** $p < 0.001$. (d) Linear regression between the SDC3 expression of monocytes and Aβ plaque loads.

Discussion

Neurodegenerative diseases, particularly Alzheimer's disease (AD), represent an urgent and growing public health challenge due to their devastating impact on cognitive function and quality of life [121,122]. Our research provides significant contributions to understanding molecular mechanisms underpinning AD pathology, with a particular focus on the roles of syndecans (SDCs) in neurodegeneration. Across five studies, we have systematically investigated the interplay between SDCs and key pathological proteins in AD, including Aβ, tau, α-syn, and ApoEs, revealing novel insights into their roles in protein aggregation, cellular uptake, and systemic inflammation.

SDCs, particularly SDC3, which are significantly overrepresented in the Alzheimer's brain, have the potential to stimulate the entry and aggregation of abnormal proteins [12,123]. In our studies, we observed that SDC3, which is found predominantly on neuronal cells, induces the most intense Aβ1-42 uptake, and the entry of these protein aggregates occurs via lipid-raft-dependent endocytosis [19]. This mechanism may contribute to the initiation of neurodegenerative processes, as fibrillation and intraneuronal accumulation of Aβ have detrimental effects on neuronal function [124]. In contrast, SDC1 and SDC2, which induce Aβ uptake to a lesser extent, show fewer pathogenic effects [24,83]. Importantly, the unique structural properties of SDC3 heparan sulfate (HS) chains and their interactions with intracellular signaling molecules have been identified as critical determinants of this process [12]. These results highlight SDC3 as a key mediator of the neuron-specific vulnerability observed in AD, where overexpression of SDC3 in human AD brains likely contributes to intraneuronal Aβ accumulation and fibrillation [12,19]. Our work emphasizes the pathogenic role of SDC3 in Aβ-induced neurotoxicity, providing a mechanistic link between its overexpression and the progression of AD. Building on the prion-like behavior of tau and α-syn, we extended our studies to elucidate the role of SDCs in the cellular uptake and spreading of these abnormal proteins [74] [24]. Our results showed that SDCs preferentially mediate the internalization of the fibrillar forms of tau and α-syn, whereas the internalization of the monomeric forms occurs mainly through SDC-independent pathways. Importantly, we have shown that SDC3 promotes the uptake of fibrillar aggregates and the fibrillation of tau and α-syn. This dual role positions SDC3 as a critical driver of protein aggregate proliferation and spreading, independent of cell type, underscoring its central role in the propagation of neurodegeneration.

The role of ApoE isoforms in AD is well established, with ApoE4 identified as a major genetic risk factor and ApoE2 as a protective factor [81]. Our study also found that different ApoE isoforms significantly affect SDC-mediated Aβ uptake [83]. The ApoE2 isoform, which reduces the risk of AD, enhances the entry of Aβ1-42 monomers into the cell, thereby decreasing its extracellular fibrillation and plaque formation, whereas ApoE4, which is associated with the highest risk, tends to inhibit this process, promoting Aβ accumulation and aggregation [83,125]. This phenomenon is particularly pronounced in the presence of the SDC3 protein, which also enhances fibrillation [83]. These findings highlight the complex and isoform-specific roles of ApoEs in amyloid pathology and underscore the importance of SDC3 as a mediator of these effects [17,83]. A particular focus is placed on SDC3, a proteoglycan that plays a role in protein aggregation and inflammation, both of which are central to AD. The role of inflammation in AD pathogenesis is increasingly recognized, and our research has further elucidated the connection between neuroinflammation and SDC3 expression [12,126]. Using in vitro and in vivo models, we demonstrated that proinflammatory cytokines, such as TNF-α, significantly upregulate SDC3 expression in neuronal-like cells and at the blood-brain barrier (BBB). This increased expression correlates with Aβ plaque burden and systemic inflammatory markers, such as elevated monocyte SDC3 levels [12]. Importantly, we identified peripheral monocyte SDC3 as a potential blood-based biomarker for AD, offering a novel diagnostic avenue that could facilitate early detection and monitoring of disease progression. Blood-based biomarkers are seen as a promising avenue, as they provide easier detection and have the potential to reveal a broader spectrum of molecular mechanisms behind AD, going beyond traditional amyloid- and tau-related markers [127]. This could not only improve diagnosis but also advance our understanding of AD pathophysiology and speed up the development of disease-modifying therapies [12,128]. Our findings also suggest that the increased expression of endothelial SDC3 at the BBB contributes to enhanced transendothelial migration of monocytes, potentially linking neuroinflammation with amyloid pathology [12,115]. This observation provides new insights into the systemic nature of AD-related inflammation. It highlights the potential utility of targeting SDC3 in therapeutic strategies to modulate inflammation and reduce amyloid burden.

Summary

In summary, our research has revealed the pivotal role of SDCs, particularly SDC3, in the molecular underpinnings of Alzheimer's disease. Through detailed analyses, we have shown that SDC3 mediates key pathological processes, including the uptake and aggregation of Aβ, tau, and α-syn, and modulates the interaction between ApoEs and amyloid pathology. Furthermore, we identified the significant upregulation of SDC3 in response to neuroinflammation and its potential as a blood-based biomarker for early AD diagnosis. These findings underscore the importance of SDC3 as both a driver of neurodegeneration and a promising target for therapeutic intervention. The logical flow of our results—from elucidating SDC3's role in protein aggregation and propagation to its involvement in inflammation and biomarker potential—provides a unified narrative that advances the understanding of AD and lays the groundwork for our future studies. The insights gained from our research contribute to a broader view of the molecular events in AD and open avenues for novel diagnostics and treatments to mitigate this disease's devastating effects.

Acknowledgments

I would like to thank my supervisor, Dr. Tamás Letoha, for his theoretical and practical guidance and the opportunity to perform the experiments in the laboratory of Pharmacoidea Ltd. in Szeged. I am also thankful to the Theoretical Medical Sciences Doctoral School of the University of Szeged for the academic framework and opportunity to pursue my PhD studies as an individual student.

References

1. Mandel, S.A.; Morelli, M.; Halperin, I.; Korczyn, A.D. Biomarkers for prediction and targeted prevention of Alzheimer's and Parkinson's diseases: evaluation of drug clinical efficacy. *EPMA J* **2010**, *1*, 273-292, doi:10.1007/s13167-010-0036-z.
2. Nussbaum, R.L.; Ellis, C.E. Alzheimer's disease and Parkinson's disease. *N Engl J Med* **2003**, *348*, 1356-1364, doi:10.1056/NEJM2003ra020003.
3. Kumar, A.; Sidhu, J.; Lui, F.; Tsao, J.W. Alzheimer Disease. In *StatPearls*; Treasure Island (FL) ineligible companies. Disclosure: Jaskirat Sidhu declares no relevant financial relationships with ineligible companies. Disclosure: Forshing Lui declares no relevant financial relationships with ineligible companies. Disclosure: Jack Tsao declares no relevant financial relationships with ineligible companies., 2025.
4. Qian, X.; Hamad, B.; Dias-Lalcaca, G. The Alzheimer disease market. *Nat Rev Drug Discov* **2015**, *14*, 675-676, doi:10.1038/nrd4749.
5. László Árpád Kostyál, Z.S., Virág Erzsébet Almási, Paolo Fabbietti, Sabrina Quattrini, Marco Socci, Giovanni Lamura, Cristina Gagliardi. Impact of the COVID-19 Pandemic on Family Carers of Older People Living with Dementia in Italy and Hungary. **2021**, doi:10.3390/su13137107.
6. Tahami Monfared, A.A.; Byrnes, M.J.; White, L.A.; Zhang, Q. Alzheimer's Disease: Epidemiology and Clinical Progression. *Neurol Ther* **2022**, *11*, 553-569, doi:10.1007/s40120-022-00338-8.
7. Wimo, A.; Seeher, K.; Cataldi, R.; Cyhlarova, E.; Dielemann, J.L.; Frisell, O.; Guerchet, M.; Jonsson, L.; Malaha, A.K.; Nichols, E.; et al. The worldwide costs of dementia in 2019. *Alzheimers Dement* **2023**, *19*, 2865-2873, doi:10.1002/alz.12901.
8. Maresova, P.; Komarkova, L.; Kuhnova, J.; Cimler, R.; Pazitny, P.; Kandilaki, D.; Musilek, K.; Truhlarova, Z.; Zemek, F.; Kuca, K. Anticipated Social and Healthcare Economic Burden of People with Alzheimer's Disease in Two Selected Regions of the Czech Republic. *Healthcare (Basel)* **2020**, *8*, doi:10.3390/healthcare8040433.
9. Passeri, E.; Elkhoury, K.; Morsink, M.; Broersen, K.; Linder, M.; Tamayol, A.; Malaplate, C.; Yen, F.T.; Arab-Tehrany, E. Alzheimer's Disease: Treatment Strategies and Their Limitations. *Int J Mol Sci* **2022**, *23*, doi:10.3390/ijms232213954.
10. Yiannopoulou, K.G.; Papageorgiou, S.G. Current and Future Treatments in Alzheimer Disease: An Update. *J Cent Nerv Syst Dis* **2020**, *12*, 1179573520907397, doi:10.1177/1179573520907397.
11. Cao, Y.; Xu, Y.; Cao, M.; Chen, N.; Zeng, Q.; Lai, M.K.P.; Fan, D.; Sethi, G.; Cao, Y. Fluid-based biomarkers for neurodegenerative diseases. *Ageing Res Rev* **2025**, 102739, doi:10.1016/j.arr.2025.102739.
12. Hudak, A.; Letoha, A.; Vizler, C.; Letoha, T. Syndecan-3 as a Novel Biomarker in Alzheimer's Disease. *Int J Mol Sci* **2022**, *23*, doi:10.3390/ijms23063407.
13. Porsteinsson, A.P.; Isaacson, R.S.; Knox, S.; Sabbagh, M.N.; Rubino, I. Diagnosis of Early Alzheimer's Disease: Clinical Practice in 2021. *J Prev Alzheimers Dis* **2021**, *8*, 371-386, doi:10.14283/jpad.2021.23.
14. Humpel, C. Identifying and validating biomarkers for Alzheimer's disease. *Trends Biotechnol* **2011**, *29*, 26-32, doi:10.1016/j.tibtech.2010.09.007.
15. Dhauria, M.; Mondal, R.; Deb, S.; Shome, G.; Chowdhury, D.; Sarkar, S.; Benito-Leon, J. Blood-Based Biomarkers in Alzheimer's Disease: Advancing Non-Invasive Diagnostics and Prognostics. *Int J Mol Sci* **2024**, *25*, doi:10.3390/ijms252010911.
16. Guo, F.; Liu, X.; Cai, H.; Le, W. Autophagy in neurodegenerative diseases: pathogenesis and therapy. *Brain Pathol* **2018**, *28*, 3-13, doi:10.1111/bpa.12545.

17. Hudák Anett, L.T. Endocytic Pathways Unveil the Role of Syndecans in the Seeding and Spreading of Pathological Protein Aggregates: Insights into Neurodegenerative Disorders. *International Journal of Molecular Sciences* **2025**, doi:10.3390/ijms26094037.
18. Gulisano, W.; Maugeri, D.; Baltrons, M.A.; Fa, M.; Amato, A.; Palmeri, A.; D'Adamio, L.; Grassi, C.; Devanand, D.P.; Honig, L.S.; et al. Role of Amyloid-beta and Tau Proteins in Alzheimer's Disease: Confuting the Amyloid Cascade. *J Alzheimers Dis* **2018**, *64*, S611-S631, doi:10.3233/JAD-179935.
19. Letoha, T.; Hudak, A.; Kusz, E.; Pettko-Szandtner, A.; Domonkos, I.; Josvay, K.; Hofmann-Apitius, M.; Szilak, L. Contribution of syndecans to cellular internalization and fibrillation of amyloid-beta(1-42). *Sci Rep* **2019**, *9*, 1393, doi:10.1038/s41598-018-37476-9.
20. Negi, S.; Khurana, N.; Duggal, N. The misfolding mystery: alpha-synuclein and the pathogenesis of Parkinson's disease. *Neurochem Int* **2024**, *177*, 105760, doi:10.1016/j.neuint.2024.105760.
21. Gallea, J.I.; Celej, M.S. Structural insights into amyloid oligomers of the Parkinson disease-related protein alpha-synuclein. *J Biol Chem* **2014**, *289*, 26733-26742, doi:10.1074/jbc.M114.566695.
22. Chen, G.F.; Xu, T.H.; Yan, Y.; Zhou, Y.R.; Jiang, Y.; Melcher, K.; Xu, H.E. Amyloid beta: structure, biology and structure-based therapeutic development. *Acta Pharmacol Sin* **2017**, *38*, 1205-1235, doi:10.1038/aps.2017.28.
23. Kim, S.; Jung, U.J.; Kim, S.R. Role of Oxidative Stress in Blood-Brain Barrier Disruption and Neurodegenerative Diseases. *Antioxidants (Basel)* **2024**, *13*, doi:10.3390/antiox13121462.
24. Hudak, A.; Kusz, E.; Domonkos, I.; Josvay, K.; Kodamullil, A.T.; Szilak, L.; Hofmann-Apitius, M.; Letoha, T. Contribution of syndecans to cellular uptake and fibrillation of alpha-synuclein and tau. *Sci Rep* **2019**, *9*, 16543, doi:10.1038/s41598-019-53038-z.
25. Davis, A.A.; Leyns, C.E.G.; Holtzman, D.M. Intercellular Spread of Protein Aggregates in Neurodegenerative Disease. *Annu Rev Cell Dev Biol* **2018**, *34*, 545-568, doi:10.1146/annurev-cellbio-100617-062636.
26. Costanzo, M.; Zurzolo, C. The cell biology of prion-like spread of protein aggregates: mechanisms and implication in neurodegeneration. *Biochem J* **2013**, *452*, 1-17, doi:10.1042/BJ20121898.
27. Antonio Blanco, G.B. Chapter 11 - Membranes. *Medical Biochemistry (Second Edition)* **2022**, doi:10.1016/B978-0-323-91599-1.00028-6.
28. Hivare, P.; Mujmer, K.; Swarup, G.; Gupta, S.; Bhatia, D. Endocytic pathways of pathogenic protein aggregates in neurodegenerative diseases. *Traffic* **2023**, *24*, 434-452, doi:10.1111/tra.12906.
29. El-Sayed, A.; Harashima, H. Endocytosis of gene delivery vectors: from clathrin-dependent to lipid raft-mediated endocytosis. *Mol Ther* **2013**, *21*, 1118-1130, doi:10.1038/mt.2013.54.
30. Steiner, J.A.; Angot, E.; Brundin, P. A deadly spread: cellular mechanisms of alpha-synuclein transfer. *Cell Death Differ* **2011**, *18*, 1425-1433, doi:10.1038/cdd.2011.53.
31. Finkbeiner, S. The Autophagy Lysosomal Pathway and Neurodegeneration. *Cold Spring Harb Perspect Biol* **2020**, *12*, doi:10.1101/cshperspect.a033993.
32. van Weering, J.R.T.; Scheper, W. Endolysosome and Autolysosome Dysfunction in Alzheimer's Disease: Where Intracellular and Extracellular Meet. *CNS Drugs* **2019**, *33*, 639-648, doi:10.1007/s40263-019-00643-1.
33. Christianson, H.C.; Belting, M. Heparan sulfate proteoglycan as a cell-surface endocytosis receptor. *Matrix Biol* **2014**, *35*, 51-55, doi:10.1016/j.matbio.2013.10.004.
34. Maiza, A.; Chantepie, S.; Vera, C.; Fifre, A.; Huynh, M.B.; Stettler, O.; Ouidja, M.O.; Papy-Garcia, D. The role of heparan sulfates in protein aggregation and their potential impact on neurodegeneration. *FEBS Lett* **2018**, *592*, 3806-3818, doi:10.1002/1873-3468.13082.
35. Sarrazin, S.; Lamanna, W.C.; Esko, J.D. Heparan sulfate proteoglycans. *Cold Spring Harb Perspect Biol* **2011**, *3*, doi:10.1101/cshperspect.a004952.

36. Cohlberg, J.A.; Li, J.; Uversky, V.N.; Fink, A.L. Heparin and other glycosaminoglycans stimulate the formation of amyloid fibrils from alpha-synuclein in vitro. *Biochemistry* **2002**, *41*, 1502-1511, doi:10.1021/bi011711s.
37. Tumova, S.; Woods, A.; Couchman, J.R. Heparan sulfate chains from glypican and syndecans bind the Hep II domain of fibronectin similarly despite minor structural differences. *J Biol Chem* **2000**, *275*, 9410-9417, doi:10.1074/jbc.275.13.9410.
38. Liu, C.C.; Zhao, N.; Yamaguchi, Y.; Cirrito, J.R.; Kanekiyo, T.; Holtzman, D.M.; Bu, G. Neuronal heparan sulfates promote amyloid pathology by modulating brain amyloid-beta clearance and aggregation in Alzheimer's disease. *Sci Transl Med* **2016**, *8*, 332ra344, doi:10.1126/scitranslmed.aad3650.
39. Yasunari Matsuzaka, R.Y. Classification and Molecular Functions of Heparan Sulfate Proteoglycans and Their Molecular Mechanisms with the Receptor. *Biologics* **2024**, doi:10.3390/biologics4020008.
40. Filmus, J. The function of glypicans in the mammalian embryo. *Am J Physiol Cell Physiol* **2022**, *322*, C694-C698, doi:10.1152/ajpcell.00045.2022.
41. Kamimura, K.; Maeda, N. Glypicans and Heparan Sulfate in Synaptic Development, Neural Plasticity, and Neurological Disorders. *Front Neural Circuits* **2021**, *15*, 595596, doi:10.3389/fncir.2021.595596.
42. Sosa, L.J.; Caceres, A.; Dupraz, S.; Oksdath, M.; Quiroga, S.; Lorenzo, A. The physiological role of the amyloid precursor protein as an adhesion molecule in the developing nervous system. *J Neurochem* **2017**, *143*, 11-29, doi:10.1111/jnc.14122.
43. Cheng, F.; Fransson, L.A.; Mani, K. Interplay between glypican-1, amyloid-beta and tau phosphorylation in human neural stem cells. *Neuroscience* **2024**, *553*, 121-127, doi:10.1016/j.neuroscience.2024.07.005.
44. Rahman, M.M.; Lendel, C. Extracellular protein components of amyloid plaques and their roles in Alzheimer's disease pathology. *Mol Neurodegener* **2021**, *16*, 59, doi:10.1186/s13024-021-00465-0.
45. Shrivastava, A.N.; Aperia, A.; Melki, R.; Triller, A. Physico-Pathologic Mechanisms Involved in Neurodegeneration: Misfolded Protein-Plasma Membrane Interactions. *Neuron* **2017**, *95*, 33-50, doi:10.1016/j.neuron.2017.05.026.
46. Kim, C.W.; Goldberger, O.A.; Gallo, R.L.; Bernfield, M. Members of the syndecan family of heparan sulfate proteoglycans are expressed in distinct cell-, tissue-, and development-specific patterns. *Mol Biol Cell* **1994**, *5*, 797-805, doi:10.1091/mbc.5.7.797.
47. Motta, J.M.; Hassan, H.; Ibrahim, S.A. Revisiting the Syndecans: Master Signaling Regulators with Prognostic and Targetable Therapeutic Values in Breast Carcinoma. *Cancers (Basel)* **2023**, *15*, doi:10.3390/cancers15061794.
48. Gopal, S.; Arokiasamy, S.; Pataki, C.; Whiteford, J.R.; Couchman, J.R. Syndecan receptors: pericellular regulators in development and inflammatory disease. *Open Biol* **2021**, *11*, 200377, doi:10.1098/rsob.200377.
49. Afratis, N.A.; Nikitovic, D.; Multhaupt, H.A.; Theocharis, A.D.; Couchman, J.R.; Karamanos, N.K. Syndecans - key regulators of cell signaling and biological functions. *FEBS J* **2017**, *284*, 27-41, doi:10.1111/febs.13940.
50. Karamanos, N.K.; Piperigkou, Z.; Theocharis, A.D.; Watanabe, H.; Franchi, M.; Baud, S.; Brezillon, S.; Gotte, M.; Passi, A.; Vigetti, D.; et al. Proteoglycan Chemical Diversity Drives Multifunctional Cell Regulation and Therapeutics. *Chem Rev* **2018**, *118*, 9152-9232, doi:10.1021/acs.chemrev.8b00354.
51. Shi, D.; Sheng, A.; Chi, L. Glycosaminoglycan-Protein Interactions and Their Roles in Human Disease. *Front Mol Biosci* **2021**, *8*, 639666, doi:10.3389/fmolb.2021.639666.
52. Lambaerts, K.; Wilcox-Adelman, S.A.; Zimmermann, P. The signaling mechanisms of syndecan heparan sulfate proteoglycans. *Curr Opin Cell Biol* **2009**, *21*, 662-669, doi:10.1016/j.ceb.2009.05.002.

53. Letoha, T.; Keller-Pinter, A.; Kusz, E.; Kolozsi, C.; Bozso, Z.; Toth, G.; Vizler, C.; Olah, Z.; Szilak, L. Cell-penetrating peptide exploited syndecans. *Biochim Biophys Acta* **2010**, *1798*, 2258-2265, doi:10.1016/j.bbamem.2010.01.022.
54. Tkachenko, E.; Simons, M. Clustering induces redistribution of syndecan-4 core protein into raft membrane domains. *J Biol Chem* **2002**, *277*, 19946-19951, doi:10.1074/jbc.M200841200.
55. Delenclos, M.; Trendafilova, T.; Mahesh, D.; Baine, A.M.; Moussaud, S.; Yan, I.K.; Patel, T.; McLean, P.J. Investigation of Endocytic Pathways for the Internalization of Exosome-Associated Oligomeric Alpha-Synuclein. *Front Neurosci* **2017**, *11*, 172, doi:10.3389/fnins.2017.00172.
56. Bayati, A.; McPherson, P.S. Alpha-synuclein, autophagy-lysosomal pathway, and Lewy bodies: Mutations, propagation, aggregation, and the formation of inclusions. *J Biol Chem* **2024**, *300*, 107742, doi:10.1016/j.jbc.2024.107742.
57. Brunello, C.A.; Merezhko, M.; Uronen, R.L.; Huttunen, H.J. Mechanisms of secretion and spreading of pathological tau protein. *Cell Mol Life Sci* **2020**, *77*, 1721-1744, doi:10.1007/s00018-019-03349-1.
58. Woods, A. Syndecans: transmembrane modulators of adhesion and matrix assembly. *J Clin Invest* **2001**, *107*, 935-941, doi:10.1172/JCI12802.
59. Carey, D.J. Syndecans: multifunctional cell-surface co-receptors. *Biochem J* **1997**, *327 (Pt 1)*, 1-16, doi:10.1042/bj3270001.
60. Turnbull, J.; Powell, A.; Guimond, S. Heparan sulfate: decoding a dynamic multifunctional cell regulator. *Trends Cell Biol* **2001**, *11*, 75-82, doi:10.1016/s0962-8924(00)01897-3.
61. Kato, M.; Wang, H.; Bernfield, M.; Gallagher, J.T.; Turnbull, J.E. Cell surface syndecan-1 on distinct cell types differs in fine structure and ligand binding of its heparan sulfate chains. *J Biol Chem* **1994**, *269*, 18881-18890.
62. Asundi, V.K.; Carey, D.J. Self-association of N-syndecan (syndecan-3) core protein is mediated by a novel structural motif in the transmembrane domain and ectodomain flanking region. *J Biol Chem* **1995**, *270*, 26404-26410, doi:10.1074/jbc.270.44.26404.
63. McFall, A.J.; Rapraeger, A.C. Identification of an adhesion site within the syndecan-4 extracellular protein domain. *J Biol Chem* **1997**, *272*, 12901-12904, doi:10.1074/jbc.272.20.12901.
64. Tkachenko, E.; Lutgens, E.; Stan, R.V.; Simons, M. Fibroblast growth factor 2 endocytosis in endothelial cells proceed via syndecan-4-dependent activation of Rac1 and a Cdc42-dependent macropinocytic pathway. *J Cell Sci* **2004**, *117*, 3189-3199, doi:10.1242/jcs.01190.
65. Jones, E.M.; Dubey, M.; Camp, P.J.; Vernon, B.C.; Biernat, J.; Mandelkow, E.; Majewski, J.; Chi, E.Y. Interaction of tau protein with model lipid membranes induces tau structural compaction and membrane disruption. *Biochemistry* **2012**, *51*, 2539-2550, doi:10.1021/bi201857v.
66. Girardot, N.; Allinquant, B.; Langui, D.; Laquerriere, A.; Dubois, B.; Hauw, J.J.; Duyckaerts, C. Accumulation of flotillin-1 in tangle-bearing neurones of Alzheimer's disease. *Neuropathol Appl Neurobiol* **2003**, *29*, 451-461, doi:10.1046/j.1365-2990.2003.00479.x.
67. Chen, Y.; Gotte, M.; Liu, J.; Park, P.W. Microbial subversion of heparan sulfate proteoglycans. *Mol Cells* **2008**, *26*, 415-426.
68. Garcia, B.; Merayo-Lloves, J.; Martin, C.; Alcalde, I.; Quiros, L.M.; Vazquez, F. Surface Proteoglycans as Mediators in Bacterial Pathogens Infections. *Front Microbiol* **2016**, *7*, 220, doi:10.3389/fmicb.2016.00220.
69. Szilak, L.; Letoha, T.; Ughy, B. What is the potential of syndecan-4-targeted novel delivery technologies? *Ther Deliv* **2013**, *4*, 1479-1481, doi:10.4155/tde.13.112.
70. Ziegler, A.; Seelig, J. Binding and clustering of glycosaminoglycans: a common property of mono- and multivalent cell-penetrating compounds. *Biophys J* **2008**, *94*, 2142-2149, doi:10.1529/biophysj.107.113472.

71. Guo, J.L.; Lee, V.M. Cell-to-cell transmission of pathogenic proteins in neurodegenerative diseases. *Nat Med* **2014**, *20*, 130-138, doi:10.1038/nm.3457.
72. Brundin, P.; Melki, R.; Kopito, R. Prion-like transmission of protein aggregates in neurodegenerative diseases. *Nat Rev Mol Cell Biol* **2010**, *11*, 301-307, doi:10.1038/nrm2873.
73. Holmes, B.B.; DeVos, S.L.; Kfoury, N.; Li, M.; Jacks, R.; Yanamandra, K.; Ouidja, M.O.; Brodsky, F.M.; Marasa, J.; Bagchi, D.P.; et al. Heparan sulfate proteoglycans mediate internalization and propagation of specific proteopathic seeds. *Proc Natl Acad Sci U S A* **2013**, *110*, E3138-3147, doi:10.1073/pnas.1301440110.
74. Holmes, B.B.; Diamond, M.I. Prion-like properties of Tau protein: the importance of extracellular Tau as a therapeutic target. *J Biol Chem* **2014**, *289*, 19855-19861, doi:10.1074/jbc.R114.549295.
75. Kfoury, N.; Holmes, B.B.; Jiang, H.; Holtzman, D.M.; Diamond, M.I. Trans-cellular propagation of Tau aggregation by fibrillar species. *J Biol Chem* **2012**, *287*, 19440-19451, doi:10.1074/jbc.M112.346072.
76. Spillantini, M.G.; Tolnay, M.; Love, S.; Goedert, M. Microtubule-associated protein tau, heparan sulphate and alpha-synuclein in several neurodegenerative diseases with dementia. *Acta Neuropathol* **1999**, *97*, 585-594, doi:10.1007/s004010051034.
77. Nguyen, D.L.B.; Okolicsanyi, R.K.; Haupt, L.M. Heparan sulfate proteoglycans: Mediators of cellular and molecular Alzheimer's disease pathogenic factors via tunnelling nanotubes? *Mol Cell Neurosci* **2024**, *129*, 103936, doi:10.1016/j.mcn.2024.103936.
78. Wang, J.; Chen, P.; Hu, B.; Cai, F.; Xu, Q.; Pan, S.; Wu, Y.; Song, W. Distinct effects of SDC3 and FGFRL1 on selective neurodegeneration in AD and PD. *FASEB J* **2023**, *37*, e22773, doi:10.1096/fj.202201359R.
79. Bartlett, A.H.; Hayashida, K.; Park, P.W. Molecular and cellular mechanisms of syndecans in tissue injury and inflammation. *Mol Cells* **2007**, *24*, 153-166.
80. Eustace, A.D.; McNaughton, E.F.; King, S.; Kehoe, O.; Kungl, A.; Mattey, D.; Nobbs, A.H.; Williams, N.; Middleton, J. Soluble syndecan-3 binds chemokines, reduces leukocyte migration in vitro and ameliorates disease severity in models of rheumatoid arthritis. *Arthritis Res Ther* **2019**, *21*, 172, doi:10.1186/s13075-019-1939-2.
81. Kim, J.; Basak, J.M.; Holtzman, D.M. The role of apolipoprotein E in Alzheimer's disease. *Neuron* **2009**, *63*, 287-303, doi:10.1016/j.neuron.2009.06.026.
82. Fernandez-Calle, R.; Konings, S.C.; Frontinan-Rubio, J.; Garcia-Revilla, J.; Camprubi-Ferrer, L.; Svensson, M.; Martinson, I.; Boza-Serrano, A.; Venero, J.L.; Nielsen, H.M.; et al. APOE in the bullseye of neurodegenerative diseases: impact of the APOE genotype in Alzheimer's disease pathology and brain diseases. *Mol Neurodegener* **2022**, *17*, 62, doi:10.1186/s13024-022-00566-4.
83. Hudak, A.; Josvay, K.; Domonkos, I.; Letoha, A.; Szilak, L.; Letoha, T. The Interplay of Apoes with Syndecans in Influencing Key Cellular Events of Amyloid Pathology. *Int J Mol Sci* **2021**, *22*, doi:10.3390/ijms22137070.
84. Fortea, J.; Pegueroles, J.; Alcolea, D.; Belbin, O.; Dols-Icardo, O.; Vaque-Alcazar, L.; Videla, L.; Gispert, J.D.; Suarez-Calvet, M.; Johnson, S.C.; et al. APOE4 homozygozity represents a distinct genetic form of Alzheimer's disease. *Nat Med* **2024**, *30*, 1284-1291, doi:10.1038/s41591-024-02931-w.
85. Verghese, P.B.; Castellano, J.M.; Garai, K.; Wang, Y.; Jiang, H.; Shah, A.; Bu, G.; Frieden, C.; Holtzman, D.M. ApoE influences amyloid-beta (Abeta) clearance despite minimal apoE/Abeta association in physiological conditions. *Proc Natl Acad Sci U S A* **2013**, *110*, E1807-1816, doi:10.1073/pnas.1220484110.
86. Kanekiyo, T.; Xu, H.; Bu, G. ApoE and Abeta in Alzheimer's disease: accidental encounters or partners? *Neuron* **2014**, *81*, 740-754, doi:10.1016/j.neuron.2014.01.045.

87. Lee, C.Y.; Tse, W.; Smith, J.D.; Landreth, G.E. Apolipoprotein E promotes beta-amyloid trafficking and degradation by modulating microglial cholesterol levels. *J Biol Chem* **2012**, *287*, 2032-2044, doi:10.1074/jbc.M111.295451.
88. Hejie Li; Wang, Z. Blood biomarkers for clinical applications in Alzheimer's disease: A narrative review. **2025**, doi:10.1016/j.neumar.2025.100078.
89. Letoha, T.; Kolozsi, C.; Ekes, C.; Keller-pinter, A.; Kusz, E.; Szakonyi, G.; Duda, E.; Szilak, L. Contribution of syndecans to lipoplex-mediated gene delivery. *Eur J Pharm Sci* **2013**, *49*, 550-555, doi:10.1016/j.ejps.2013.05.022.
90. Kovalevich, J.; Langford, D. Considerations for the use of SH-SY5Y neuroblastoma cells in neurobiology. *Methods Mol Biol* **2013**, *1078*, 9-21, doi:10.1007/978-1-62703-640-5_2.
91. Ihse, E.; Yamakado, H.; van Wijk, X.M.; Lawrence, R.; Esko, J.D.; Masliah, E. Cellular internalization of alpha-synuclein aggregates by cell surface heparan sulfate depends on aggregate conformation and cell type. *Sci Rep* **2017**, *7*, 9008, doi:10.1038/s41598-017-08720-5.
92. Busetto, S.; Trevisan, E.; Patriarca, P.; Menegazzi, R. A single-step, sensitive flow cytofluorometric assay for the simultaneous assessment of membrane-bound and ingested Candida albicans in phagocytosing neutrophils. *Cytometry A* **2004**, *58*, 201-206, doi:10.1002/cyto.a.20014.
93. Nakase, I.; Tadokoro, A.; Kawabata, N.; Takeuchi, T.; Katoh, H.; Hiramoto, K.; Negishi, M.; Nomizu, M.; Sugiura, Y.; Futaki, S. Interaction of arginine-rich peptides with membrane-associated proteoglycans is crucial for induction of actin organization and macropinocytosis. *Biochemistry* **2007**, *46*, 492-501, doi:10.1021/bi0612824.
94. Xue, C.; Lin, T.Y.; Chang, D.; Guo, Z. Thioflavin T as an amyloid dye: fibril quantification, optimal concentration and effect on aggregation. *R Soc Open Sci* **2017**, *4*, 160696, doi:10.1098/rsos.160696.
95. Assmann, J.C.; Muller, K.; Wenzel, J.; Walther, T.; Brands, J.; Thornton, P.; Allan, S.M.; Schwaninger, M. Isolation and Cultivation of Primary Brain Endothelial Cells from Adult Mice. *Bio Protoc* **2017**, *7*, doi:10.21769/BioProtoc.2294.
96. Wesen, E.; Jeffries, G.D.M.; Matson Dzebo, M.; Esbjorner, E.K. Endocytic uptake of monomeric amyloid-beta peptides is clathrin- and dynamin-independent and results in selective accumulation of Abeta(1-42) compared to Abeta(1-40). *Sci Rep* **2017**, *7*, 2021, doi:10.1038/s41598-017-02227-9.
97. Attisano, L.; Wrana, J.L.; Lopez-Casillas, F.; Massague, J. TGF-beta receptors and actions. *Biochim Biophys Acta* **1994**, *1222*, 71-80, doi:10.1016/0167-4889(94)90026-4.
98. Shi, W.; Bartlett, J.S. RGD inclusion in VP3 provides adeno-associated virus type 2 (AAV2)-based vectors with a heparan sulfate-independent cell entry mechanism. *Mol Ther* **2003**, *7*, 515-525, doi:10.1016/s1525-0016(03)00042-x.
99. Shafti-Keramat, S.; Handisurya, A.; Kriehuber, E.; Meneguzzi, G.; Slupetzky, K.; Kirnbauer, R. Different heparan sulfate proteoglycans serve as cellular receptors for human papillomaviruses. *J Virol* **2003**, *77*, 13125-13135, doi:10.1128/jvi.77.24.13125-13135.2003.
100. Libeu, C.P.; Lund-Katz, S.; Phillips, M.C.; Wehrli, S.; Hernaiz, M.J.; Capila, I.; Linhardt, R.J.; Raffai, R.L.; Newhouse, Y.M.; Zhou, F.; et al. New insights into the heparan sulfate proteoglycan-binding activity of apolipoprotein E. *J Biol Chem* **2001**, *276*, 39138-39144, doi:10.1074/jbc.M104746200.
101. Yamauchi, Y.; Deguchi, N.; Takagi, C.; Tanaka, M.; Dhanasekaran, P.; Nakano, M.; Handa, T.; Phillips, M.C.; Lund-Katz, S.; Saito, H. Role of the N- and C-terminal domains in binding of apolipoprotein E isoforms to heparan sulfate and dermatan sulfate: a surface plasmon resonance study. *Biochemistry* **2008**, *47*, 6702-6710, doi:10.1021/bi8003999.
102. R.W., M. Remnant lipoprotein metabolism: Key pathways involving cell-surface heparan sulfate proteoglycans and apolipoprotein E. *Journal of Lipid Research* **1999**, doi:10.1016/S0022-2275(20)33334-4.

103. Dunn, K.W.; Kamocka, M.M.; McDonald, J.H. A practical guide to evaluating colocalization in biological microscopy. *Am J Physiol Cell Physiol* **2011**, *300*, C723-742, doi:10.1152/ajpcell.00462.2010.
104. Manders, E.M.; Stap, J.; Brakenhoff, G.J.; van Driel, R.; Aten, J.A. Dynamics of three-dimensional replication patterns during the S-phase, analysed by double labelling of DNA and confocal microscopy. *J Cell Sci* **1992**, *103 (Pt 3)*, 857-862, doi:10.1242/jcs.103.3.857.
105. Adler, J.; Parmryd, I. Quantifying colocalization by correlation: the Pearson correlation coefficient is superior to the Mander's overlap coefficient. *Cytometry A* **2010**, *77*, 733-742, doi:10.1002/cyto.a.20896.
106. Encinas, M.; Iglesias, M.; Liu, Y.; Wang, H.; Muhaisen, A.; Cena, V.; Gallego, C.; Comella, J.X. Sequential treatment of SH-SY5Y cells with retinoic acid and brain-derived neurotrophic factor gives rise to fully differentiated, neurotrophic factor-dependent, human neuron-like cells. *J Neurochem* **2000**, *75*, 991-1003, doi:10.1046/j.1471-4159.2000.0750991.x.
107. Agholme, L.; Lindstrom, T.; Kagedal, K.; Marcusson, J.; Hallbeck, M. An in vitro model for neuroscience: differentiation of SH-SY5Y cells into cells with morphological and biochemical characteristics of mature neurons. *J Alzheimers Dis* **2010**, *20*, 1069-1082, doi:10.3233/JAD-2010-091363.
108. Tsiolaki, P.L.; Katsafana, A.D.; Baltoumas, F.A.; Louros, N.N.; Iconomidou, V.A. Hidden Aggregation Hot-Spots on Human Apolipoprotein E: A Structural Study. *Int J Mol Sci* **2019**, *20*, doi:10.3390/ijms20092274.
109. Carter, D.B. The interaction of amyloid-beta with ApoE. *Subcell Biochem* **2005**, *38*, 255-272, doi:10.1007/0-387-23226-5_13.
110. Liu, C.C.; Zhao, N.; Fu, Y.; Wang, N.; Linares, C.; Tsai, C.W.; Bu, G. ApoE4 Accelerates Early Seeding of Amyloid Pathology. *Neuron* **2017**, *96*, 1024-1032 e1023, doi:10.1016/j.neuron.2017.11.013.
111. Cao, J.; Hou, J.; Ping, J.; Cai, D. Advances in developing novel therapeutic strategies for Alzheimer's disease. *Mol Neurodegener* **2018**, *13*, 64, doi:10.1186/s13024-018-0299-8.
112. Arokiasamy, S.; Balderstone, M.J.M.; De Rossi, G.; Whiteford, J.R. Syndecan-3 in Inflammation and Angiogenesis. *Front Immunol* **2019**, *10*, 3031, doi:10.3389/fimmu.2019.03031.
113. Patterson, A.M.; Gardner, L.; Shaw, J.; David, G.; Loreau, E.; Aguilar, L.; Ashton, B.A.; Middleton, J. Induction of a CXCL8 binding site on endothelial syndecan-3 in rheumatoid synovium. *Arthritis Rheum* **2005**, *52*, 2331-2342, doi:10.1002/art.21222.
114. Patterson, A.M.; Cartwright, A.; David, G.; Fitzgerald, O.; Bresnihan, B.; Ashton, B.A.; Middleton, J. Differential expression of syndecans and glypicans in chronically inflamed synovium. *Ann Rheum Dis* **2008**, *67*, 592-601, doi:10.1136/ard.2006.063875.
115. Floris, S.; van den Born, J.; van der Pol, S.M.; Dijkstra, C.D.; De Vries, H.E. Heparan sulfate proteoglycans modulate monocyte migration across cerebral endothelium. *J Neuropathol Exp Neurol* **2003**, *62*, 780-790, doi:10.1093/jnen/62.7.780.
116. Di Bona, D.; Candore, G.; Franceschi, C.; Licastro, F.; Colonna-Romano, G.; Camma, C.; Lio, D.; Caruso, C. Systematic review by meta-analyses on the possible role of TNF-alpha polymorphisms in association with Alzheimer's disease. *Brain Res Rev* **2009**, *61*, 60-68, doi:10.1016/j.brainresrev.2009.05.001.
117. Weksler, B.; Romero, I.A.; Couraud, P.O. The hCMEC/D3 cell line as a model of the human blood brain barrier. *Fluids Barriers CNS* **2013**, *10*, 16, doi:10.1186/2045-8118-10-16.
118. Lewis, J.; Dickson, D.W.; Lin, W.L.; Chisholm, L.; Corral, A.; Jones, G.; Yen, S.H.; Sahara, N.; Skipper, L.; Yager, D.; et al. Enhanced neurofibrillary degeneration in transgenic mice expressing mutant tau and APP. *Science* **2001**, *293*, 1487-1491, doi:10.1126/science.1058189.
119. Newman, P.J. The biology of PECAM-1. *J Clin Invest* **1997**, *100*, S25-29.

120. Kapellos, T.S.; Bonaguro, L.; Gemund, I.; Reusch, N.; Saglam, A.; Hinkley, E.R.; Schultze, J.L. Human Monocyte Subsets and Phenotypes in Major Chronic Inflammatory Diseases. *Front Immunol* **2019**, *10*, 2035, doi:10.3389/fimmu.2019.02035.
121. Wang, S.; Jiang, Y.; Yang, A.; Meng, F.; Zhang, J. The Expanding Burden of Neurodegenerative Diseases: An Unmet Medical and Social Need. *Aging Dis* **2024**, doi:10.14336/AD.2024.1071.
122. Wortmann, M. Dementia: a global health priority - highlights from an ADI and World Health Organization report. *Alzheimers Res Ther* **2012**, *4*, 40, doi:10.1186/alzrt143.
123. Lorente-Gea, L.; Garcia, B.; Martin, C.; Ordiales, H.; Garcia-Suarez, O.; Pina-Batista, K.M.; Merayo-Lloves, J.; Quiros, L.M.; Fernandez-Vega, I. Heparan Sulfate Proteoglycans Undergo Differential Expression Alterations in Alzheimer Disease Brains. *J Neuropathol Exp Neurol* **2020**, *79*, 474-483, doi:10.1093/jnen/nlaa016.
124. Bayer, T.A.; Wirths, O. Intracellular accumulation of amyloid-Beta - a predictor for synaptic dysfunction and neuron loss in Alzheimer's disease. *Front Aging Neurosci* **2010**, *2*, 8, doi:10.3389/fnagi.2010.00008.
125. Raulin, A.C.; Doss, S.V.; Trottier, Z.A.; Ikezu, T.C.; Bu, G.; Liu, C.C. ApoE in Alzheimer's disease: pathophysiology and therapeutic strategies. *Mol Neurodegener* **2022**, *17*, 72, doi:10.1186/s13024-022-00574-4.
126. Azizi, G.; Navabi, S.S.; Al-Shukaili, A.; Seyedzadeh, M.H.; Yazdani, R.; Mirshafiey, A. The Role of Inflammatory Mediators in the Pathogenesis of Alzheimer's Disease. *Sultan Qaboos Univ Med J* **2015**, *15*, e305-316, doi:10.18295/squmj.2015.15.03.002.
127. Hansson, O.; Blennow, K.; Zetterberg, H.; Dage, J. Blood biomarkers for Alzheimer's disease in clinical practice and trials. *Nat Aging* **2023**, *3*, 506-519, doi:10.1038/s43587-023-00403-3.
128. Pais, M.; Martinez, L.; Ribeiro, O.; Loureiro, J.; Fernandez, R.; Valiengo, L.; Canineu, P.; Stella, F.; Talib, L.; Radanovic, M.; et al. Early diagnosis and treatment of Alzheimer's disease: new definitions and challenges. *Braz J Psychiatry* **2020**, *42*, 431-441, doi:10.1590/1516-4446-2019-0735.